UNIVERSIDAD DE LAS PALMAS DE GRAN CANARIA
Instituto Universitario de Microelectrónica Aplicada
Sistemas de información y Comunicaciones

Máster en
Tecnologías de Telecomunicación

IUMA

Trabajo Fin de Máster

Técnicas de Reconocimiento Automático de Patrones Aplicadas a Imágenes Hiperespectrales Médicas

Autor: **Samuel Ortega Sarmiento**
Tutor(es): **Dr. Gustavo Marrero Callicó**
D. Rafael Camacho Galán
Fecha: **septiembre - 2016**

IUMA
t +34 928 451 086
f +34 928 451 083
iuma@iuma.ulpgc.es
www.iuma.ulpgc.es
Campus Universitario de Tafira
35017 Las Palmas de Gran Canaria

Versión: 2.0 – 14 jun 2011

UNIVERSIDAD DE LAS PALMAS DE GRAN CANARIA
Instituto Universitario de Microelectrónica Aplicada
Sistemas de información y Comunicaciones

Máster en
Tecnologías de Telecomunicación

Trabajo Fin de Máster

Técnicas de Reconocimiento Automático de Patrones Aplicadas a Imágenes Hiperespectrales Médicas

HOJA DE FIRMAS

Alumno/a: Samuel Ortega Sarmiento Fdo.:

Tutor/a: Dr. Gustavo Marrero Callicó Fdo.:

Tutor/a: D. Rafael Camacho Galán Fdo.: P.O.

Fecha: septiembre - 2016

Versión: 2.0 – 14 jun 2011

UNIVERSIDAD DE LAS PALMAS DE GRAN CANARIA
Instituto Universitario de Microelectrónica Aplicada
Sistemas de información y Comunicaciones

Máster en
Tecnologías de Telecomunicación

IUMA

Trabajo Fin de Máster

Técnicas de Reconocimiento Automático de Patrones Aplicadas a Imágenes Hiperespectrales Médicas

HOJA DE EVALUACIÓN

Calificación: ....

Presidente: Fdo.:

Secretario: Fdo.:

Vocal: Fdo.:

Fecha: septiembre - 2016

IUMA
t +34 928 451 086
f +34 928 451 083
iuma@iuma.ulpgc.es
www.iuma.ulpgc.es
Campus Universitario de Tafira
35017 Las Palmas de Gran Canaria

Versión: 2.0 – 14 jun 2011

Agradecimientos

En primer lugar, me gustaría dar las gracias a mi tutor, Gustavo Marrero, por haber confiado en mí y haberme dado una oportunidad que me ha permitido formar parte de este grupo de investigación. También quiero agradecer a todos mis compañeros del grupo de investigación que me hayan aguantado durante esta etapa de mi vida. Creo que somos un buen grupo que se complementa muy bien y espero que sigamos así durante mucho tiempo. Especialmente agradezco a Himar su paciencia conmigo en ciertos momentos duros.

Y como no, gracias a mi familia y a mis amigos, que dan sentido a mi vida fuera del contexto académico.

Index

Figures

Tables

Summary

Hyperspectral imaging is an emerging technology for medical diagnosis. Some previous studies have employed this technology for detecting cancer diseases. In this research work, a multidisciplinary team compounds by pathologists and engineers present a proof of concept of using hyperspectral imaging analysis in order to detect human brain tumour tissue inside pathological slides. The samples were acquired from four different patient diagnosed with brain cancer, specifically with high-grade gliomas. The hyperspectral capture system consists on a hyperspectral camera coupled with a microscope. This system works in the VNIR spectral range (from 400 nm to 1000 nm) with a spectral resolution of 3 nm. The images where then processed in order to remove the effect caused by the acquisition system. Later, and based on the diagnostic provided by pathologist, a spectral dataset containing only labelled spectra from normal and tumour tissue was created.

The data were then processed using three different supervised learning algorithms: Support Vector Machines, Artificial Neural Networks and Random Forests. The capabilities of discriminating between normal and tumour tissue have been evaluated in three different scenarios, where the inter-patient variability of data was or not taken into account. The results achieved in this research study are promising, showing that it is possible to distinguish between normal and tumour tissue exclusively attending to the spectral signature of tissue.

Resumen

Las imágenes hiperespectrales son una tecnología emergente en el campo de la medicina debido a su capacidad de detectar la composición química de distintos materiales de forma no invasiva. Algunos estudios previos ya han empleado esta tecnología para la detección de cáncer. En este trabajo de investigación, un equipo multidisciplinar compuestos por patólogos e ingenieros presentan una prueba de concepto donde se emplea el análisis de imágenes hiperespectrales con el fin de detectar tejido tumoral en muestras histológicas. Las muestras usadas en este estudio han sido obtenidas de cuatro pacientes diferentes a los que han diagnosticado previamente cáncer cerebral, más específicamente gliomas de alto grado. El sistema de captura hiperespectral consiste en una cámara hiperespectral acoplada a un microscopio. Este sistema funciona en el rango espectral VNIR (de 400 nm a 1000 nm) con una resolución espectral de 3 nm. Las imágenes se han procesado con el fin de eliminar cualquier efecto causado por el sistema de adquisición, independizando la medida del sistema de captura. A continuación, y tomando como base en el diagnóstico proporcionado por los patólogos, se ha creado una base de datos que contiene únicamente la información espectral de cada tejido y la etiqueta que define el diagnostico de cada tipo de tejido (sano o tumoral).

Los datos se han procesado utilizando tres algoritmos de aprendizaje supervisado diferentes: Support Vector Machines, Redes Neuronales Artificiales y Random Forests. Las capacidades de discriminación entre tejido normal y tumoral se han evaluado en tres escenarios diferentes, donde la variabilidad inter-paciente de los datos ha sido o no tenida en cuenta. Los resultados obtenidos en este estudio de investigación son prometedores, mostrando que es posible distinguir entre el tejido normal y tumoral exclusivamente atendiendo a la firma espectral del tejido.

Chapter 1: Introduction

1.1 Context

The main motivation to carry out this project is the European Project HELICOID: Hyperspectral Imaging Cancer Detection (FP7-618080) from IUMA. This project, with Dr. Gustavo Marrero Callicó as the principal investigator (PI), has the main goal of applying hyperspectral imaging techniques for the precise identification of malignant tumours during surgical procedures. The HELICoiD project aims to develop an experimental intraoperative setup based on non-invasive hyperspectral cameras connected to a platform running a set of algorithms capable of discriminating between healthy or tumour tissues.

On the other hand, to understand the context of this project it is necessary to know that the Integrated System Design Division, DSI, from IUMA is specialized in the treatment of hyperspectral images. DSI team has already undergoing projects such as:

CCSDS Lossless Compression IP-core Space Applications (ITT-No. AO/1-8032/14/NL/AK)

The main objective of this ITT (invitation to Tender) is to implement two separate IP-cores corresponding to the CCSDS 123 and CCSDS 121 standards respectively. The former corresponds to a Lossless Multispectral and Hyperspectral Image Compression architecture, while latter is a Lossless Data Compressor. Both IP-cores will be mapped for space qualified FPGAs (from Microsemi and Xilinx) and also for radiation hardened standard cells (180 nm ATMEL ATC18RHA).

REBECCA: Resilient Embedded Electronic Systems for Controlling Cities under Atypical Situations (TEC2014-58036-C4-4-R)

REBECCA is oriented to the Smart City paradigm. This topic brings up important challenges in different areas related with the sustainable development of the city and the provision of services to citizens. Among these areas, REBECCA focuses on urban security for large public spaces and/or celebration of major events. In this context, REBECCA works on the design of a platform for sensing and distributed computing of visible and multi-hyper-spectral image processing.

ENABLE-S3: European initiative to Enable Validation for Highly Automated Safe and Secure Systems

ENABLE-S3 is a strongly industry-driven project. It will pave the way for accelerated application of highly automated and autonomous systems in the mobility domains automotive, aerospace, rail, maritime and health, through provision of highly effective test and validation methodology and platforms. ENBALE-S· will help the European industry to gain leadership in the strategic field of autonomous systems due to faster development and test of new products.

HYLOC: Multispectral and Hyperspectral Image Compression System

The objective of this industrial project is the implementation of a prototype suitable for its implementation on a space-qualified FPGA for the compression of multispectral and hyperspectral images based on the standard CCSDS-123. The effect of the several configuration parameters on the compression efficiency and hardware complexity is taken into consideration to provide flexibility in such a way that the implementation can be adapted to different applications scenarios.

1.2 Objectives

GLOBAL OBJECTIVES

The main objective of this Master's Thesis is to propose and validate several classification models and use data mining techniques in order to obtain an automatic diagnostic tool for medical hyperspectral imaging. These hyperspectral images consist on captures from histological samples from healthy brain tissue and tumour previously diagnosed by a pathologist in the VNIR (400nm - 1000nm) spectral range.

OPERATIVE OBJECTIVES

- Understand the nature of the hyperspectral data in order to exploit correctly the main features of the available dataset. Knowing the main techniques for processing the hyperspectral imaging, their applications and studying the most-suitable data mining techniques for processing this kind of data.
- Propose different frameworks for processing and classifying hyperspectral data, using different classification schemes and processing techniques.
- Evaluate the performance of the proposed frameworks and decide which of them are most suitable for distinguishing between healthy and tumour tissue.

1.3 Methodology

The methodology followed in this research work is related with the previously described objectives. This methodology can be summarized as follows. First, the documentation regarding hyperspectral images have been analysed, playing special attention to the use of this technology in the medical field. Then, a supervised classification framework is proposed in order to automatically distinguish between normal and tumour tissue using the spectral signature of tissue. Some scenarios have been proposed to evaluate the performance of the model. These scenarios take or not into account the inter-patient variability of data. Finally, the classification results obtained by each classifier for each scenario have been evaluated.

1.4 Document Overview

This document is organized as follows:

Chapter 1: The first chapter of this document consists on a brief introduction to the research work that will be described in this document. This chapter covers the context where this research work is developed, the objectives and a brief description of the methodology followed in order to achieve the objectives.

Chapter 2: In this chapter, an introduction to the hyperspectral images is provided. This introduction covers the basic concepts of this technology, the most relevant processing techniques that are usually applied to this kind of data and the main applications where the hyperspectral images are useful. Finally, a review of the state of art involving medical hyperspectral imaging is presented and the basic concepts of supervised learning algorithms are provided.

Chapter 3: This chapter presents the materials employed in this research work, where the database employed in this research work is described. This dataset has been acquired from pathological slides that have been previously analysed by pathologist after brain tumour surgeries. This chapter also describes the foundations of the proposed processing techniques employed to extract knowledge from hyperspectral data.

Chapter 4: In this part of the document the results obtained after processing the hyperspectral images are shown.

Chapter 5: The last chapter sums up the conclusions achieved during the growth of this research work. Also the on-going work is described.

Chapter 2: State of Art

2.1 Hyperspectral Imaging

Hyperspectral Imaging (HSI), also known as imaging spectroscopy [1], is a technology capable of acquiring hundreds of contiguous spectral bands for a given scene. HSI is the combination of two technologies: spectroscopy and digital imaging. On the one hand, spectroscopy is the field that deals about the interaction between the electromagnetic radiation and matter. Meanwhile, digital imaging cares about acquiring snapshots from a scene. Therefore, HSI simultaneously captures the spatial and spectral properties from the materials inside a scene.

The interest of this imaging technique is given by the fact that the interaction between the electromagnetic radiation of light with a given material is singular for that material. The measured spectrum from a given material is called spectral signature, and throw the analysis of this wavelength-dependent function it is possible to discriminate between different types of materials. An example of different spectral signatures belonging to different materials is shown in Figure 1. The reflectance spectrum in Figure 1 shows the spectral signature of three different materials (soil, water and green vegetation) from 400nm to 2500nm. It can be observed that it is possible to differentiate between different materials uniquely attending to their spectral signature.

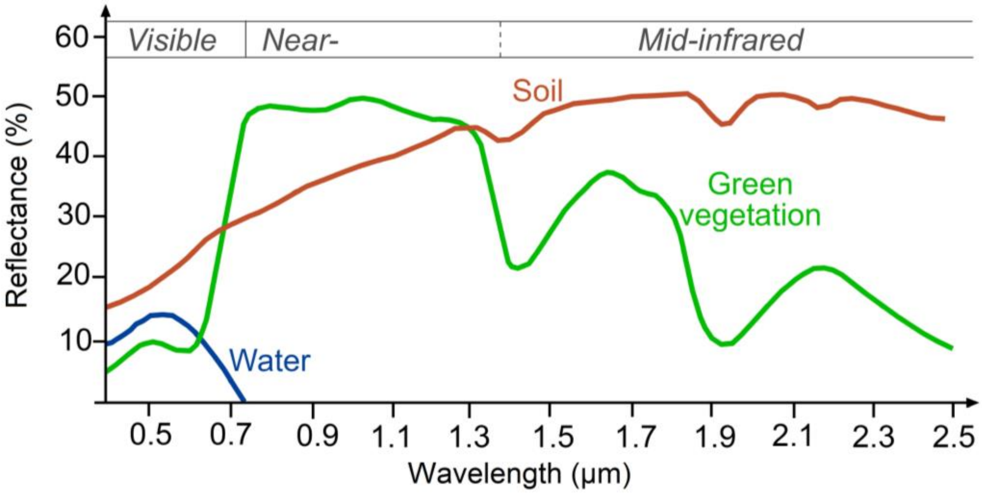

Figure 1: Spectral signature of different materials

In order to handle the vocabulary that refers to hyperspectral images, some definitions must be provided. The digital representation of a hyperspectral image is called **hypercube**, and it stores both the spatial and spectral information (Figure 2.a). One pixel in the hyperspectral image corresponds to the spectrum from a certain spatial coordinate (Figure 2.b). The **spectral range** of a hyperspectral image is the portion of the electromagnetic spectrum that has been sampled when acquiring the hypercube. There are several standard values for the spectral range from 400nm to 2500nm, each spectral region is fitted to a certain application. For example, mineralogy applications use the spectral range from 1000nm to 2500nm, since vegetation analysis can be performed in the 400nm to 1000nm range. The **spectral resolution** refers to the maximum number of spectral bands that can be resolved by a hyperspectral camera. For example, if we have a hyperspectral camera working in the VNIR spectral range (from 400nm to 600nm), if the spectral resolution is 1nm, the camera is capable to discriminate between 600 hundred different spectral bands; controversy if the spectral resolution were 3nm the camera will be able to acquire 200 bands. Finally, the **spatial resolution** is defined as the size of the smallest object that can be recorded by the camera. It is an important feature depending on the application, for instance, urban area mapping requires sufficient spatial resolution to distinguish small spectral classes, such as cars in a street.

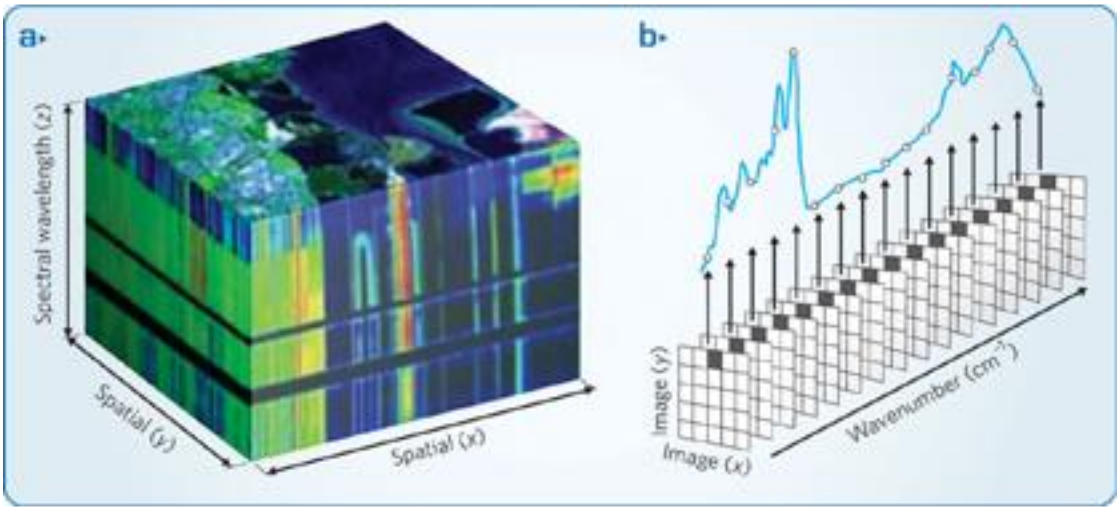

Figure 2: Hypercube that stores the HSI

In order to provide the reader with a briefly but robust context to hyperspectral images, this chapter presents the current trends in applications and digital image processing of hyperspectral images.

2.1.1 Hyperspectral Imaging Applications

The discrimination capability between different materials provided by HSI makes this technology very attractive in a large variety of fields. This section presents an overview of several HSI applications, trying to show the powerful of this technology. Medical applications of HIS, which is the actual context of this research study, will be reviewed later in this document.

Historically, the first application of HSI was Remote Sensing. Remote Sensing deals with the acquisition and processing of data from the Earth's surface and aims to extract knowledge from this data. The goal is to identify materials, objects or areas attending to the spectral signature recorded by a satellite or aircrafts. Remote sensing applications of hyperspectral images cover many disciplines such as hydrology, oceanography, mineralogy, precision agriculture or military applications [2]. As an example of a Remote Sensing application, in Figure 3 the results of a research study carried out at University of California are presented [3]. In this study, the discrimination between invasive plants against non-invasive plants is accomplished. It can be easily seen that the invasive plants (Iceplant) are identified and even the density of the invasive plants in each area is located.

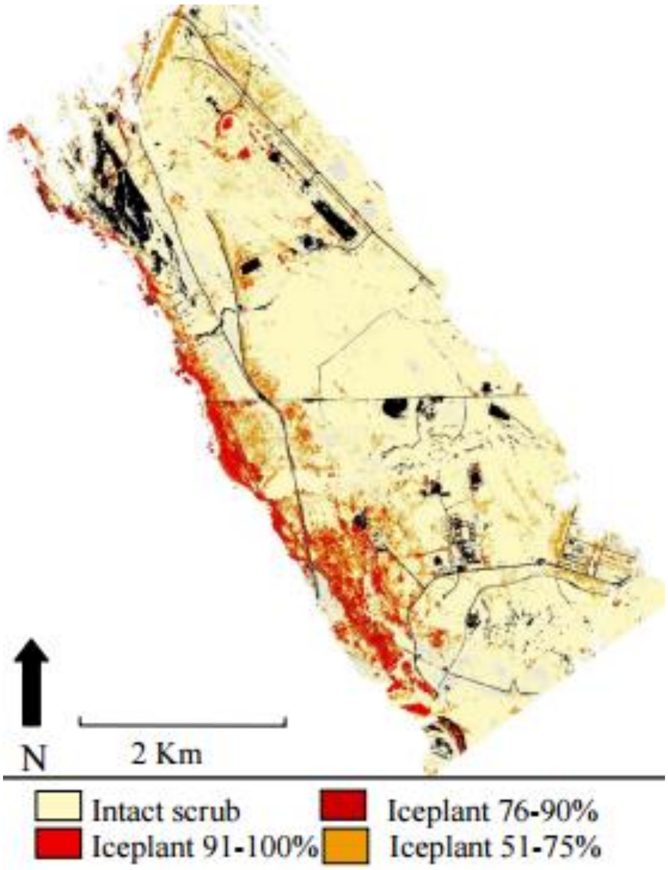

Figure 3: Invasive plants identification using HSI

On the other hand, hyperspectral imaging has emerged as a powerful tool for automated food sorting and quality assessment applications. There are many ways of assessing food quality, such as sensory evaluation or chemical methods, but generally these analytical methods are time consuming and leads to the product destruction. Therefore, these traditional methods are not compatible with large-scale productions. In this context, hyperspectral imaging has earned an important role during the recent years, proving to be an effective technique for non-destructive and fast analysis and evaluation of food products. Motivated by this reasons, hyperspectral imaging technology has been already use for quality assessment in meat, fish, fruit and vegetables [4][5]. One example of applying hyperspectral analysis in food quality assessment is presented in Figure 4 [6]. The image shows the results of identifying different defects in oranges. The defects detected are the following: insect damage (Figure 4.a), wind scarring (Figure 4.b), trips scaring (Figure 4.c), scale infestation (Figure 4.d), canker spot (Figure 4.e), copper burn (Figure 4.f), phytotoxicity (Figure 4.g), heterochromatic stripe (Figure 4.h) and stem-end (Figure 4.i).

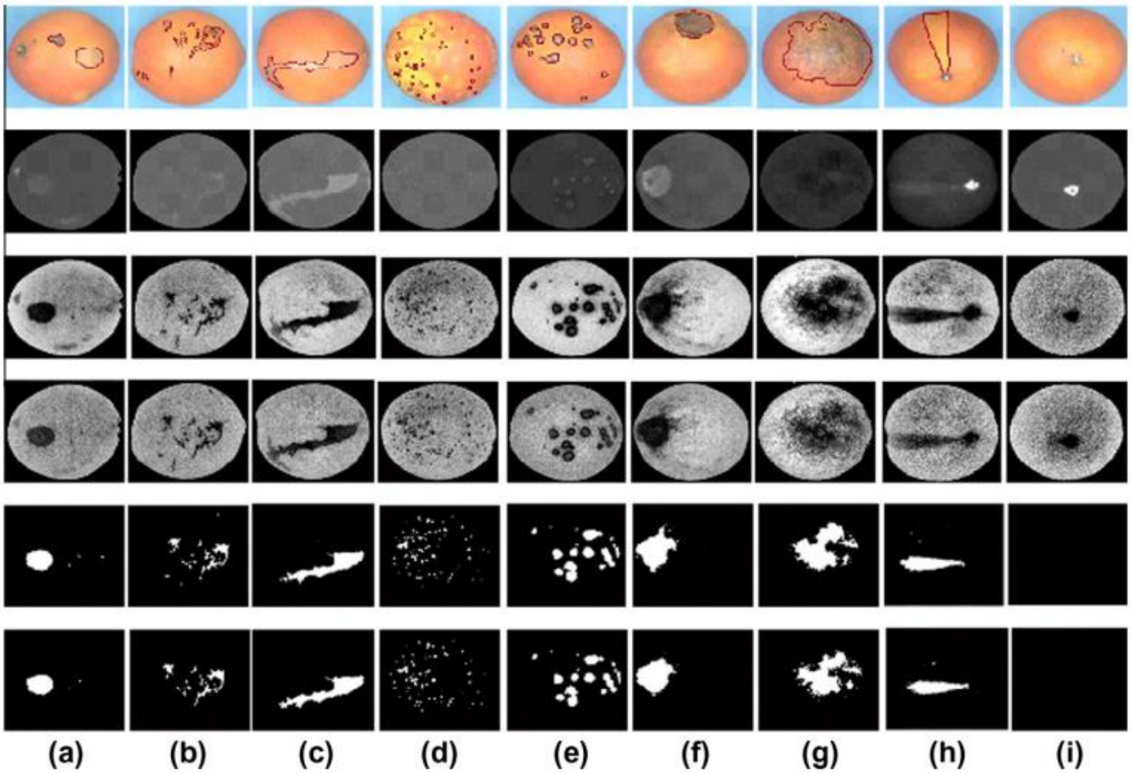

Figure 4: Detection of different defects in oranges

Hyperspectral imaging has been also employed in the pharmaceutical industry. In this field, the main goals are improving the quality control, identify drugs and detect counterfeit. Hyperspectral imaging has proven advantages compared with traditional drug analysis techniques, usually based on chemical analysis. Figure 5 shows an interesting application in the pharmaceutical field: the detection of counterfeit drugs. Counterfeit drugs do not comply with the security and safety quality standard provided by laboratories, therefore active ingredients may differ from the optimal dose quantity, causing unpredictable reactions in patients. Figure 5 (left side) shows a mixture of normal and counterfeiting pills that are hardly distinguishable to the naked eye. When processing the hyperspectral image of these drugs, it is possible to discriminate between the normal ones and the counterfeited ones (Figure 5, right side) [6].

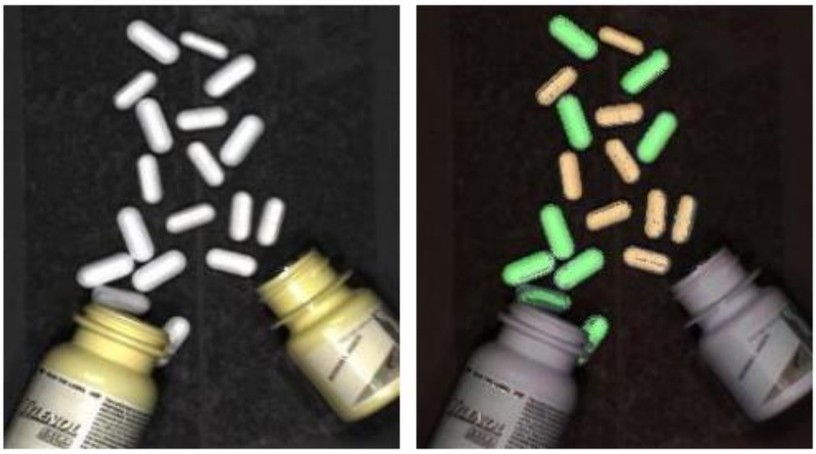

Figure 5: Detection of counterfeit drugs using HSI

This technology has also shown good opportunities in defense and security applications. Several studies have employed HSI for the detection of military targets, such as vehicles, decoys, camouflages or landmine areas [7]. Another relevant application is illustrated on Figure 6, where HSI have been applied for the identification of chemical clouds [8]. In Figure 6 the different chemicals are highlighted using different colours, and the transparency level is related with the gas concentration in each case.

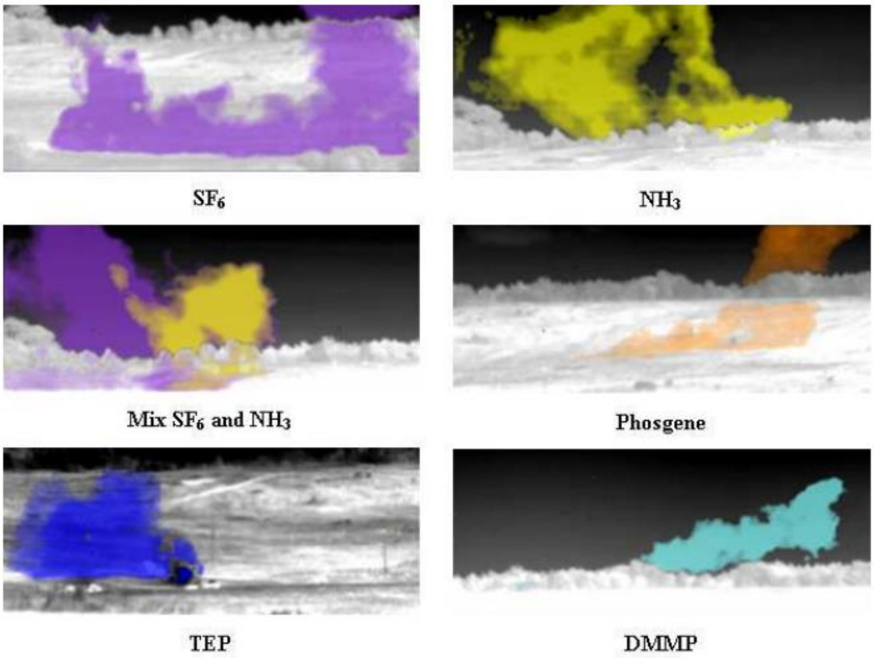

Figure 6: Chemical gases releases using HSI

2.1.2 Hyperspectral Imaging Processing

The intrinsic characteristics of hyperspectral data arise different processing issues, which must be necessarily tacked under specific mathematical formalisms, such as classification and segmentation, spectral mixture analysis, anomaly detection, target detection and data compression [9]. A briefly description of each hyperspectral image processing techniques is provided in this section.

Anomaly Detection algorithms in hyperspectral imaging aims to detect pixels in the hypercube whose spectra differ significantly from the background spectra of the hyperspectral image [10]. A variety of anomaly detection techniques that have been applied to hyperspectral images can be found in the literature.

Meanwhile, *Target Detection* applications seek to identify a relatively small number of objects with fixed spatial or spectral characteristics inside a hypercube. Many of these applications involve the detection of an object or activity such as a military vehicle or vehicle tracks [11].

Spectral mixture analysis and *spectral unmixing* techniques are motivated due to the low spatial resolution of sensors for a given application, causing that the measured spectra in a certain pixel is a mixture of various spectrum of materials in the recorded scene. Unmixing techniques are intended to estimating the number of pure-spectral materials (called endmembers), extract their spectral signatures and calculate their abundances in each pixel. Main applications of Remote Sensing employs this kind of techniques due to the relatively low resolution of the airbone sensors compared with the target size in the Earth surface. An overview of these techniques can be found on [12].

As already mentioned, the high dimensionality of multispectral and hyperspectral data is highly advantageous from the point of view of image analysis for scientific purposes. However, a challenge appears when the images are acquired on a satellite, where the amount of storage and the downlink bandwidth are limited. *Data compression* can alleviate this problem, by reducing the data volume prior to transmission to a ground station. Hyperspectral image compression has become a popular research field in the past years, and many different algorithms have been proposed for hyperspectral data compression [13].

Classification and *segmentation* of hyperspectral images consists in applying Machine Learning techniques in order to extract useful information from the hyperspectral data. Supervised classification and segmentation is an important process in hyperspectral image processing. The goal of this kind of algorithms is to automatically extract some similarity criteria that allow the discrimination between different classes based on some features. Although the first approaches regarding hyperspectral image classification uniquely exploits the spectral information of each pixel, it has been proven that the combination of both the spatial and spectral characteristics of the hyperspectral data usually improve the quality of the predictions made by the classifier. A wide range of applications such as crop monitoring, urban mapping and tracking or disease detection are actually handled by using appropriate data and efficient classifiers [14].

2.2 Medical Hyperspectral Imaging

While most traditional biomedical optical imaging methods can only capture grey or colour images of biological samples, the targets of interest in these kinds of images are generally analysed by their spatial properties such as size, shape and texture. It has been widely recognized that the monochrome and RGB colour imaging methods have limitations in the early detection and identification of tissue abnormalities.

On the other hand, through the spectroscopic diagnostic technology, it is possible to acquire an entire spectrum of a single tissue site within a wavelength region of interest. This method is usually referred to as the point measurement method, which cannot provide the spatial information of samples. According to the electromagnetic theory, different biochemical constituents commonly have different spectral signatures. These signatures are usually generated by the interactions between materials and electromagnetic waves, such as electron transition, atomic and molecular vibration or rotation. The biological and pathological changes in tissues and organs also have a close relationship with the spectra. Spectral characteristics in different wavelength regions yield a distinguishable spectral signature, making pathological changes distinguishable. Therefore, the interaction between the electromagnetic radiation and tissue carries quantitative information about tissue pathology [15].

For this reasons, hyperspectral imaging technology has been extended to the biomedical engineering field to estimate the physiological status of biological tissues, since it can take advantage of the spatial relationships among the different spectra in a neighbourhood. This technology opens new prospects for life science by which scientists can identify and quantify the relationships among biologically active molecules, observe living organisms non-invasively, perform histopathological and fluorescent analyses, and enhance biological understanding of diseases. In the past decades, researchers have developed various spectral imaging systems for the biochemical analysis of various biological organs and tissues [16].

A standard for achieving a medical hyper spectral imager system has been not yet established. Therefore, the most suitable kind of spectral acquisition systems (pushbroom, filter-based or snapshots) and their intrinsic characteristics (spectral range, spectral resolution and spatial resolution) vary in each research study. Another way of classifying medical HSI applications is attending to the diseases that are studied. Finally, different MHSI applications employ different processing techniques to extract information from the hyperspectral images. In this section, an overview of some research studies regarding the use of hyperspectral images for diagnostic issues is presented.

In section, the state-of-art of the Medical Hyperspectral Imaging is reviewed. To this end, three research groups that have been worked in hyperspectral imaging in the medical field have been analysed.

RESEARCH GROUP I: TOKYO INSTITUTE OF TECHNOLOGY

This research group is one of the pathfinders in the use of hyperspectral imaging in the medical field. Radiologist, engineers and medical doctors from USA and Japan compose this research group. Their publications are intended to find a new way for disease identification in real time.

In their first paper [17], this research group describes the use of hyperspectral images with twofold objectives: the detection of blood vessels and the differentiation between arteries and veins. The motivations are the following: first, an unexpected location of blood vessels during surgery may result in an accidental injury to the blood vessel. On the other hand, differentiating between arteries and veins is necessary in majority of medical procedure. This research work is based in experiments during abdominal surgeries carried out in pigs, where the hyperspectral images were captured using two hyperspectral cameras. One of the cameras works in the spectral range from 400 nm to 1000 nm, and the other covers the electromagnetic spectrum from 1000 nm to 1700 nm. The automatic identification of arteries and veins has been obtained using a SVM classifier. The performance on detecting arteries and veins has been shown good results for the aorta and cava vein. Figure 7 show synthetic images where the veins and arteries are remarked in red and blue colours respectively.

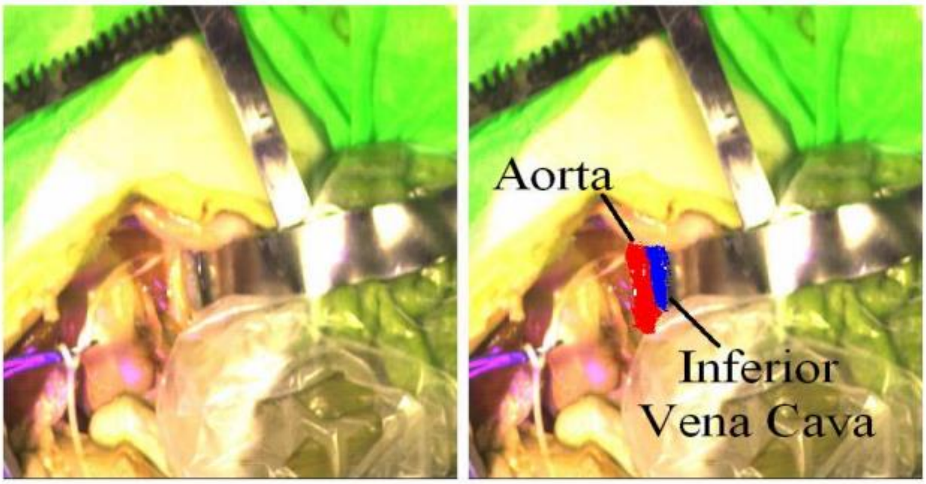

Figure 7: Identification of aorta and vena cava using HSI

In their second research work involving hyperspectral imaging [18], they applied this technology for developing and intraoperative tool capable to detect intestinal ischemia. The intestinal ischemia can be defined as an inadequate blood flow to the intestine, causing an inability to absorb food and nutrients, bloody diarrheal, infection and gangrene. The spectral signatures of the intestinal ischemia were acquired during pig abdominal surgeries. Two cameras were used, covering from 400 nm to 1700 nm. The methodology followed in this paper to process the HSI data consisted in finding an optimal normalized difference index that allow the discrimination of intestinal ischemia over other kind of tissue. The normalized index has been employed as filters for the image processing. In Figure 8 the detection of the intestinal ischemia during the time in a surgery is shown. The ischemia regions have been highlighted using a black mask. The outcome of this article concludes that the selected processing technique is suitable for detecting intestinal ischemia during surgical procedures.

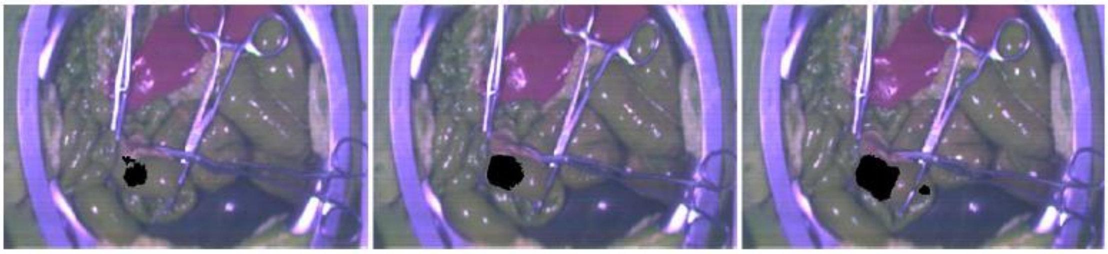

Figure 8: Ischemia detection during time using HSI

Other interesting research can be found on [19], where the authors describe the use of HSI for detecting human gastric cancer. This study was carried out over ten patients who underwent a total gastrectomy. The hyperspectral images were captured ex-vivo after the resection of tumour using a camera that covers from 1000 nm to 2500 nm. After pathologic diagnosis, the real diagnosis is compared with the image processing results. The hypercubes were processed using different techniques: a standard deviation method (that tries to enhance the difference between normal and tumour tissue), a normalized cancer difference index (NDCI) and a supervised classifier based on SVM. Attending to the image processing results (Figure 9), NDCI has been shown as the technique that better suits to the discrimination between gastric normal and tumour tissue.

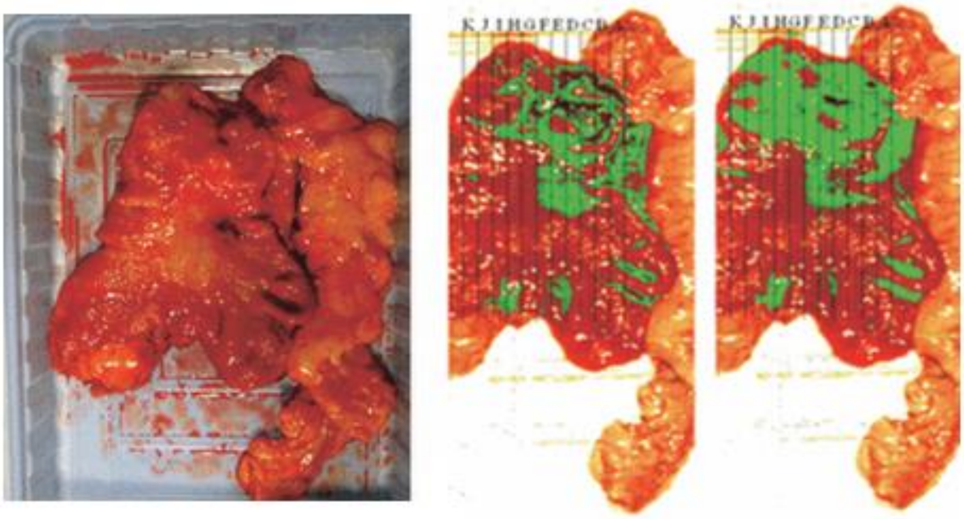

Figure 9: Gastric cancer detection using HIS. (a) RGB image (b)(c) Detected cancer areas

RESEARCH GROUP II: EMORY UNIVERSITY

One of the most active research group in biomedical applications of HSI is leaded by Professor Baowei Fei, from the Department of Biomedical Engineer at Emory University. This group has been researching about exploiting hyperspectral data since 2012. In their first research studies they collaborated with Akabari, who was working with the research group described in the previous section. The main characteristics of the HIS research performed by this group can be summarized as follows. Generally, their experiments explore cancer diseases in animal subjects. Moreover, they usually work using an LCTF-based acquisition system in the VNIR spectral range, from 400nm to 1000nm. Most of their experiments have been carried out in-vivo during surgical procedures. Due to this fact, they research has exhaustively analysed which pre-processing techniques are most suitable to compensate the variation of the environmental conditions during the acquisition. Finally, the processing techniques employed in order to extract information from the hypercubes vary depending on each research study, but each new publication present novel and more sophisticated methods. In this section, most of the publications of this research group are briefly reviewed.

The first research work using HSI [20] describes the acquisition and data processing of hyperspectral images from pathological slides. To this end, 19 mice were induced human head and neck metastatic cells. Then, once the tumour has grown, the lymph nodes and the lung tissue were histologically processed and sent to pathology. The pathological slides were captured using a LCTF hyperspectral camera working from 450 nm to 950 nm. Figure 10 shows the intensity spectra acquired for both type of tissue (lymph nodes and lung) and both cancerous and normal tissue. The spectral differences between the healthy and diseased tissue can be easily observed. The spectral data were processed using SVM, achieving good discrimination rate between normal and tumour tissue (higher than 97% of specificity and 92.6% of sensitivity). The conclusions of this study reveal that MHSI can be used as a tool that can help pathologist to detect the cancer without an exhaustive examination of slides.

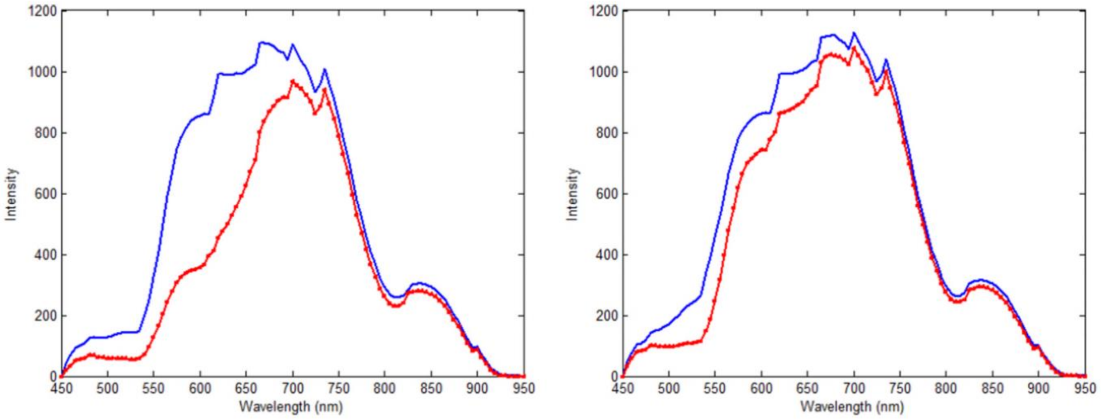

Figure 10: Measured spectra for lymph nodes and lung

In their second research work using this technology [21], the authors propose the use of hyperspectral imaging for prostate cancer detection. This study was performed over 11 mice that had human prostate tumour growing on their flaws. The HIS acquisition was performed both in-vivo (from 450 nm to 950 nm) and in-vitro (from 420nm to 720nm). The image processing consisted on a supervised classification using Support Vector Machines. The results from this study, with high specificity and sensitivity values in both experimental setups, show that HSI is a suitable technology for the automatic detection of prostate cancer. Figure 11 shows the tumour area detected after processing the hypercubes, where cancerous tissue has been highlighted using a yellow colour code.

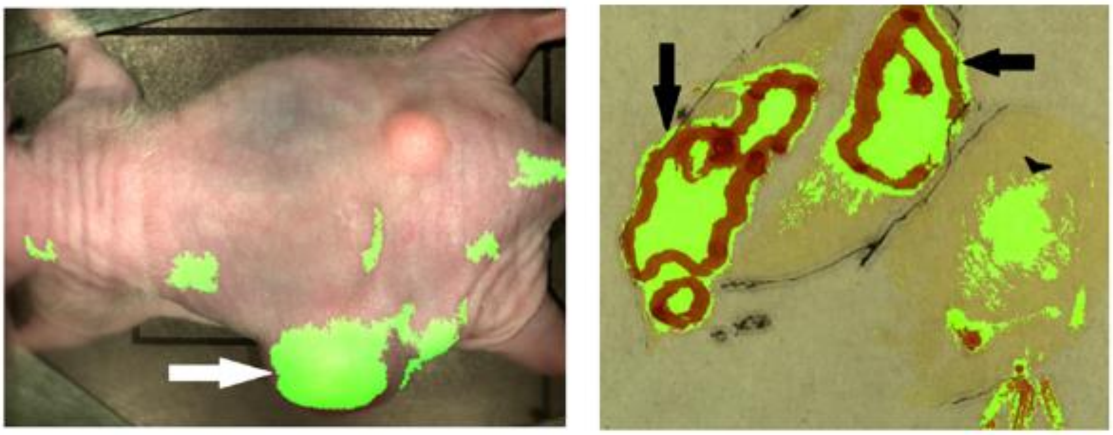

Figure 11: Prostate cancer detection, in vivo and in vitro

In [22], they explore the capability of HSI in detecting head and neck cancer. The experiments were performed over in-vivo mice that were induced head and neck tumour cells with a Green Fluorescence Protein (GFP). Tumours show green signals in fluorescence images due to tumour cells with GFP. The GFP spectral bands inside the hyperspectral images are used to delimitate the tumour and generate a golden reference map of the tumour area. These bands were removed from the hypercubes in order to avoid their influence in the classification process. Figure 12.a shows a RGB synthetic image from one hypercube. Figure 12.b shows the gold standard diagnostic of tumour and Figure 12.c presents the results of the classification process. A novel framework consisting in tensor decomposition for feature extraction and classification was proposed to face the image processing in this study. It has been proven that the proposed classification reaches a good discrimination rate between malignant and healthy tissue, enhancing other traditional pixel-wise classification methods.

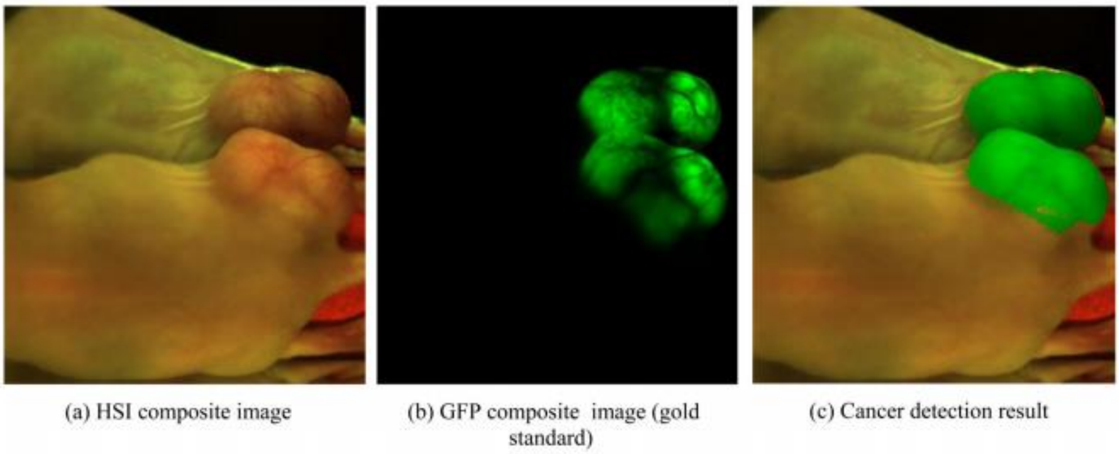

Figure 12: Head and neck cancer detection using HSI

In [23] the authors present a way to validate the tumour margins detected by HSI using histological images. The objective of this study is to relate the macroscopic HSI images with the histological microscopic images, which provide the ground truth of cancer margins. The proposed methods extract the Principal Component Analysis (PCA) from the hypercube (macroscopic) and match this image with the microscopic histological image. Figure 13 shows the results of this study. In Figure 13.a the grey-scaled histological is shown, Figure 13.b presents an RGB representation of the hypercube. Figure 13.c shows a one-band representation of the hypercube using PCA and finally Figure 13.d show an overlay of the hyperspectral image registered with the histological image. This results allows the correlation of the hypercubes with the golden reference provided by the pathological diagnosis.

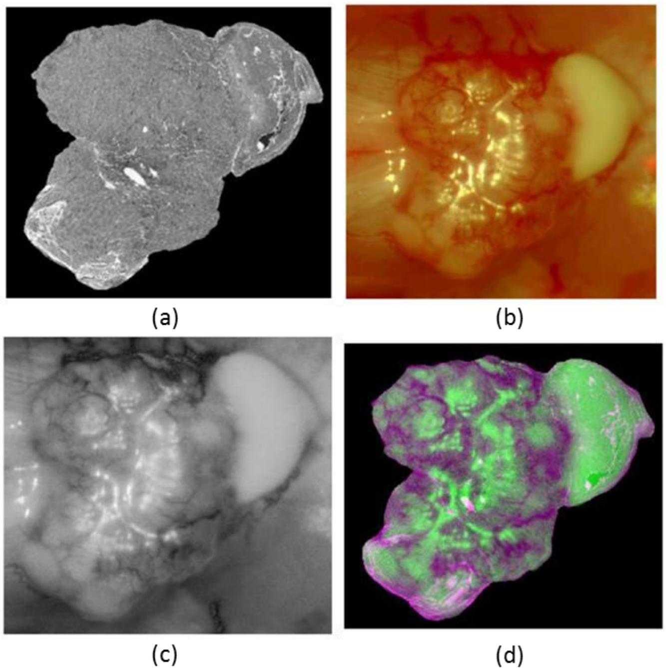

Figure 13: Histological and hyperspectral images registered

The study carried out in [24] worries about developing an aid-visualizing tool to be used by surgeons intraoperative. The study was based on experiments over mice with neck and head tumour in the spectral range from 450 nm to 950 nm. The main goal of this study is to apply a processing chain that cares about the environmental conditions inside the operation theatre. In Figure 14 the block diagram of the processing scheme is presented. First, a pre-processing chain is applied to the in-vivo acquired hypercube. This pre-processing chain takes special attention to compensate to compensate the issues discovered when capturing in-vivo HSI data in a surgical scenario: presence of glare pixel in the image and curvature correction. Glare strongly affects the appearance of intraoperative images, presenting a problem for surgical image analysis. So far, curvature correction has to be applied in order to compensate the difference in the measured intensity recorded by the camera due to the elevation of some tissues respect to another. Once the pre-processing chain has been applied, a wavelength optimization is performed in order to find a wavelength subset that optimally characterizes the difference between cancerous and normal tissue. Then, a supervised classification is performed using SVM. Finally, a spatial post-processing is performed. This HSI processing framework has shown a great capability on differentiating between normal and tumour tissue with high specificity and sensitivity.

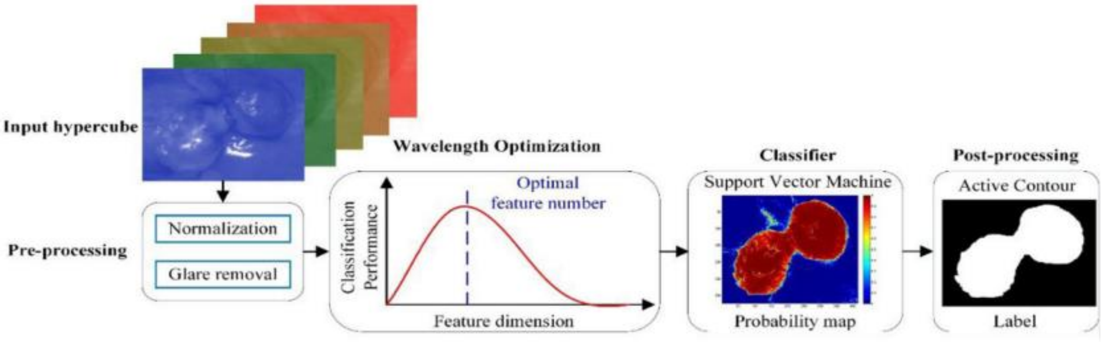

Figure 14: Proposed framework for classifying medical HSI

Another framework for processing hyperspectral images during surgical procedures is presented in [25]. The proposed novelties in this research are threefold: a robust pre-processing stage that compensate the environmental conditions during the image registration, the introduction of new features extracted from the hypercube in order to increase the information provided to a supervised classifier, and a feature selection stage capable to choose the most relevant predictors that allow an optimal discrimination between normal and tumour tissue. The pre-processing chain innovations consist in a motion correction (in order to compensate the movements in the scene during the acquisition of the hypercube) and a novel method for glare removal. Four new features have been included as new predictors together with the spectral data: the first and second order derivate of the spectral curve, statistical values extracted from the spectral curve (such as the mean, standard deviation and total reflectance at each pixel) and the Fourier Coefficients of the spectral data. In order to reduce the increased number of predictors, a feature selection method based on the Maximal Relevance and Minimum Redundancy criterion have been applied.

A method that combines both the spatial and spectral characteristics of the hyperspectral data has been recently published [26]. The proposed method combines an optimal band selection method based on a pixel-wise SVM classification with a Minimum Spanning Forest (MSF) strategy. The model has been tested through classifying data acquired from in-vivo mice that were induced with head and neck tumour. Figure 15 shows how the classification results provide an accurate prediction based on the golden reference.

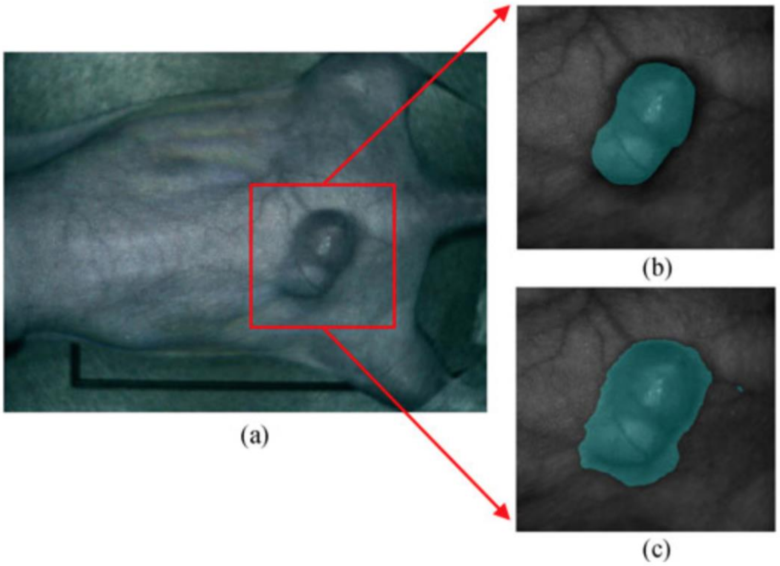

Figure 15: (a) RGB representation of mouse (b) Gold standard (c) Classification results

Finally, in a recently published paper [], this research group have presented a method for estimating skin concentrations of haemoglobin and melanin. The target application of this study is the early detection of oral cancer. The novelty introduced in this study is the processing technique that aims to apply a spectral unmixing framework in order to decompose the hyperspectral data into chromosphore concentration maps. The experiments were carried out using simulated data, phantom blood vessels and samples acquired in-vivo. The results obtained from the in-vivo dataset are shown in Figure X. The hemoglobin and melanin concentration maps have been successfully obtained.

RESEARCH GROUP III: NORWEGIAN UNIVERSITY OF SCIENCE AND TECHNOLOGY

The third research group that is analysed in this document is compound by Norway researchers. Their first investigation using HSI was in 2014. Instead of using the classical framework for processing HSI, this group have included an inverse model approximation, where the optical model of the light-tissue interaction is simulated using the Light Transport Model. Once a spectral model of the response of a certain tissue is generated, it is compared with the measured spectra using a hyperspectral camera. They usually work analysing the optical properties of skin in order to diagnose different diseases. This research group is also involved in two European projects that employ hyperspectral imaging for medical issues: SEMITOCONS [28] and IACOBUS [29]. Some of the papers published by this research work are analysed bellow:

In one of their first research work involving hyperspectral images [30], the authors aim to extract tissue properties combining an analytical model of light propagation with the real-time analysis of the hyperspectral images. To this end, the authors use an algorithm that fits the acquired hyperspectral data to an analytical skin model and extract information that can provide different tissue properties. A light transport model, that is used to obtain the diffusion reflectance as a wavelength function, was employed. The skin model proposed has two layers (Figure 16) and the tissue properties that are estimated using the inverse modelling strategy are the melanin absorption in epidermis, the oxygen saturation of blood in dermis or other chromosphores such as water or fat. The inverse modelling was evaluated using a simulated reflectance spectra composed by a four-layer skin model and a Monte Carlo simulation. The preliminary results achieved in this study are promising, but the authors found problems due to the in-vivo environmental condition variations during the acquisition of the hypercubes.

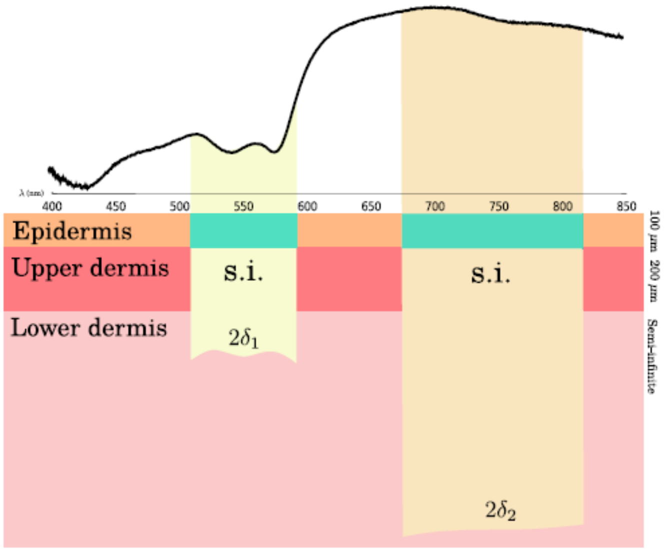

Figure 16: Two layer skin model used by [30]

In [31] the authors propose a method for detecting high cholesterol levels by analysing hyperspectral images from human facial skin. This research has been accomplished in the context of a European Project named SEMEOTICONS [28] that aims to develop a cholesterol diagnosis tool based on HSI. The first stage of this research work was preforming a numerical simulation of human skin affected by hypercholesterolemia. The skin model proposed has two layers and the simulation of the light transport in skin tissue is based on a weighted-photon Monte Carlo technique. After simulating the spectra of tissue affected by cholesterol, the authors mixed this spectrum with the hyperspectral data of human skin. Using the Minimum Noise Fraction (MNF) algorithm, the MNF-eigenvector that enhances the visualization of tissue with high cholesterol levels was found. In order to evaluate this methodology, a clinical study involving 11 volunteers with different levels of cholesterol was carried out. The images were acquired using a LCTF camera that works from 400nm to 720nm. The conclusions of this study shown that the proposed method provides good performance detecting lipid deposits, and releases that HSI is a promising technology for providing a fast diagnosis of cholesterol. Figure 17 shows the results of applying the previously described method. In Figure 17.a the information of the volunteers is shown, in Figure 17.b a synthetic RGB image from each patient. Finally Figure 17.c show the MNF transformation of the hypercubes using the eigenvector that enhances the visualization of tissue with cholesterol. In this Figure the normal cholesterol level (up to 200mg/dl) is represented in blue, the border cholesterol levels (200mg/dl – 240mg/dl) are presented in cyan and the high cholesterol levels (more than 240mg/dl) are shown in yellow.

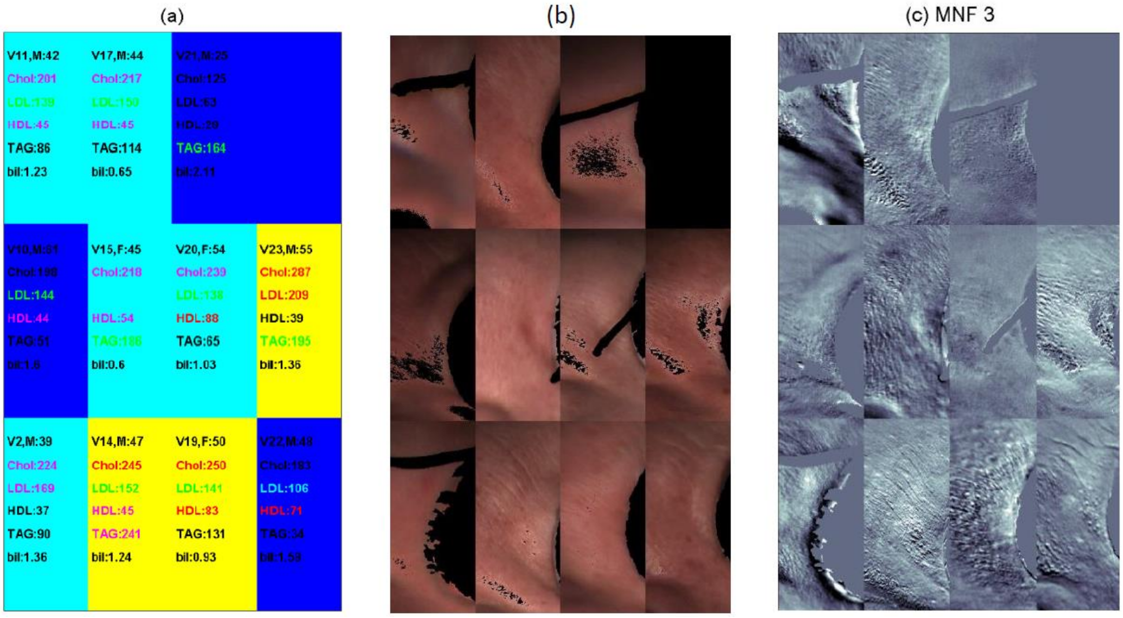

Figure 17: Detection of cholesterol using HSI

In other research work [32], the authors aim to enhance the vessel visualization using HSI. Three different methods were used in order to enhance the contrast between vessels and background tissue. Once veins have been located, an inverse model technique is applied in order to estimate the depth and oxygenation of each blood vessel. The algorithms that have been evaluated to enhance the vein contrast are the Discrete Wavelet Transform (DWT), the Minimum Noise Fraction (MNF) and an analytical inverse model. The conclusions obtained by the authors are the following: both DWT and MNF provides a clear visualization of vessels, nevertheless MNF is a statistical method which decomposition depends on the image statistics. So, the results obtained through wavelet transformation are more consistent because DWT always use the same decomposition filters. The inverse model method does not enhance the results obtained using DWT or MNF. For these reasons, wavelet transformation has been presented as the most suitable technique for vessel enhanced images. Once the blood vessels have been identified, the authors applied an inverse modelling technique for estimating the vessel oxygenation and depth, showing promising results. The results of applying this technique are presented in Figure 18, where both the identification of blood vessels and the estimation of their oxygenation levels are shown.

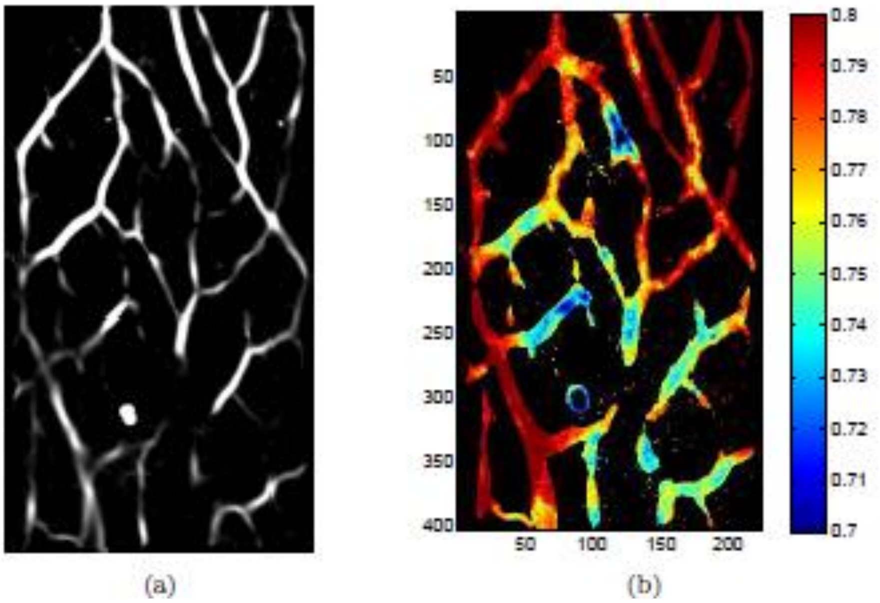

(a) (b)

Figure 18: Vessel identification (a) and oxygenation estimation (b) using hyperspectral images

The research work described in [33] aims to develop a novel imaging technique for a non-invasive diagnosis of rheumatoid arthritis. This research work is part of a European project, IACOBUS [29], and tries to find a diagnosis alternative technology for the detection of arthritis. Conventional diagnostic techniques in this field are expensive, time consuming and require trained experts who collect and interpret data. Using the information about the human finger joints physiology and anatomy was employed to construct an analytical model of human joints. In order to simulate the photon transport model, a three dimensional Monte Carlo model was used. By analysing the simulations, it has been reached that the wavelength regions from 800nm to 900nm and from 1050nm to 1100nm in light transmission mode can enhance the identification of arthritis in the human joints. It has been also concluded that the reflectance spectrum will not provide useful information for diagnosing arthritis. Although these simulations served as an important tool for understanding and developing an arthritis diagnosis tool based on HSI, and experimental study have to be carried out in order to validate the simulations.

Outside the intensively analysed research groups, there are many researchers who have employed hyperspectral images for diagnosing different diseases, but they have not been included in this state of art review. For instance, some studies worrying about the detection of tumour using HSI have explored cervical neoplasia [34], breast cancer [35], lung cancer [36], gastric cancer [37] or tongue cancer [38].

2.3 Supervised Learning

Supervised learning is a field inside Machine Learning. The goal of machine learning is to extract knowledge from experimental data and process these data in order to find patterns or for decision-making issues [39]. The Machine Learning techniques can be classified in three major groups: supervised learning, semi-supervised learning and unsupervised learning. Supervised learning algorithms employ a given set of data with known responses (labels), and generate a model that makes predictions for the response of new data. Otherwise, in unsupervised learning problems the response of each simple in the dataset is not known. The goal of unsupervised learning consists in grouping the data in different clusters based in some similarity criteria. Finally, semi-supervised learning methods use both labelled and unlabelled data to make a prediction.

In this research work supervised classification is performed over hyperspectral data in order to automatically discriminate between normal and tumour tissue. This section provides the basic concepts involved in supervised classification.

The dataset for supervised classification problems consist on n pairs (x_i, y_i), where the instances (x_i) are m-dimensional vectors $x \in R^m$ and the target values or labels (y_i) can be neither categorical values nor continuous variables. When the target variable is a categorical value the problem is called classification and when the target data is continuous the problem is called regression. The goal of supervised learning techniques is, given a training set, to learn a function that is able to predict the target value of previously unseen instances.

The common workflow in classification problems is shown in Figure 19. The first stage consists on dividing the available data into two disjoints subsets: the training set and the test set. The training set is the set of instances that is provided to the classifier in order to create an input-output relationship for prediction. The test set is employed to assess the classifier performance, and consists on previously unseen instances. After splitting data into training set and test set, it is usual to extract meaningful features from the raw data in order to facilitate the learning task to the classifier. In the training stage the train set is used to build the model, and in the prediction stage this model is evaluated using the test set.

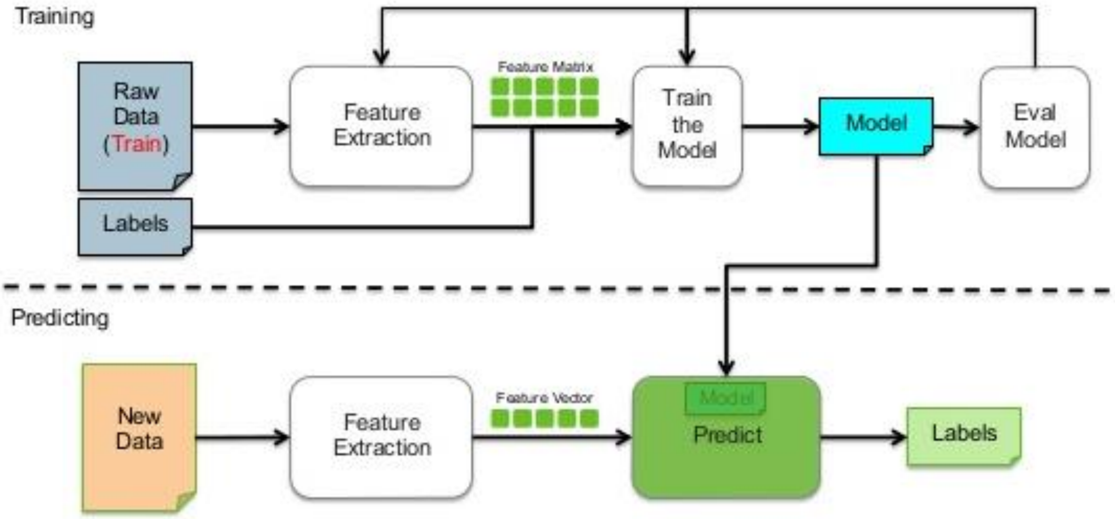

Figure 19: Standard workflow for supervised learning problems

2.4 Summary

This chapter introduces the reader to the basic knowledge about hyperspectral imaging technology, including the main processing techniques and applications. According to the context of this research work, the state of art of medical hyperspectral images have been explored. The work from three different research groups with a contrasted trajectory dealing with medical hyperspectral images, have been carefully analysed. Finally, a brief introduction to the basic concepts involving supervised classifiers have been presented.

Chapter 3: Materials and Methods

3.1 Biological samples description

In this research study all patients are affected by glioblastoma multiforme. Malignant gliomas are most common form of primary brain tumours in adults with a high incidence that it is between 11-12/100000 person per year in USA [40][41]. The three most frequent type of glioma are glioblastoma multiforme (GBM), anaplastic astrocytoma (AA) and anaplastic oligodendroglioma (AO). Gliomas cause between the 2% and 3% of cancer deaths in the whole world [40]. This type of tumours has in common their glial origin and their prevalent location is the supratentorial region. Gliomas can appear in any age range, but mainly affect adults between 45 and 70 years old [42]. GBM is the most frequent tumour, around 30% of the cases, and the most aggressive with a mean of 10 to 15 month of survival and a diagnostic mean age is 56 years old. AA and AO are less frequent, around 20% and 7% of the cases respectively, and they can appear at early mean ages, around 45 years old, and a high survival time [42][44]. This type of tumours mainly uses the white matter of the brain or the cerebrospinal fluid to be disseminated and, unlike the other types of advanced malignant neoplasm, they are no characterized by expanded and generate distant metastasis.

The most frequent clinical presentation of glioblastoma multiforme patients is a slowly progressive neurological deficit, typically subacute, with motor weakness, being the most common headache symptoms (50%) [45]. This symptom can appear in a holocraneal non-specific character profile or with intracranial hypertension. Between 30% and 50% of the patients present focal motor symptoms or signs and around 60% present cognitive impairment to the diagnosis. Finally, only between 15% and 20% of the patients manifest seizures.

There are many factors that can be associated to the survival increasing of the patient, such as, secondary gliomas through tumour progression, the early age of the patient, a highly preoperative Karnofsky score (KPS) and a suitable surgical and oncological treatment [46]. In this last factor, the radical resection together with the radiotherapy and temozolomide administration is associated with a better survival rates.

The dataset employed in this study have been previously acquired in another research work [47]. The biological samples used in this research work consist in biopsies from human brain tissue resected during surgery. A sample of the tumour's tissue is required for the pathologic diagnosis during or after the surgery. A biopsy is the removal of a small amount of tissue for the examination under a microscope and is the conclusive way that a brain tumour can be trustworthy diagnosed. The sample removed during the biopsy is analysed by a pathologist. A biopsy can be done as part of a surgery to remove the entire tumour or as a separate procedure if surgical removal of the tumour is not possible because of its location or patient's health. This biopsy has followed a histological processing, whereby tissue specimens are prepared for sectioning, staining and diagnosis. Once biopsy has been diagnosed, tissue is sorted according to the Wold Health Organization (WHO) classification of tumours of the nervous system.

Figure 20: Biological samples

In this study, 4 different patients were analysed, and 13 diagnosed pathological slides were available (Figure 20, left side). These pathology slides were provided by the Anatomy Pathology department of Doctor Negrín Hospital, at Las Palmas of Gran Canaria.

In order to facilitate the labelling process of the hyperspectral data, once pathologists had a diagnosis for a certain tissue, they marked the regions of interest in the slide with a coloured pen. Tumour tissues were marked using red colour, and healthy tissues were marked using blue colour (Figure 20, right side).

3.2 Acquisition system

In order to register hyperspectral images from pathology slides, an acquisition system consisting on a HSI camera coupled with a microscope has been employed (Figure 21, left side). The hyperspectral camera used was the Specim ImSpector VNIR V10-E, which works in the VNIR spectral range (from 400 nm to 1000 nm) with a spectral resolution of 2.8 nm. It is a pushbroom camera, so to capture a whole hypercube, either the camera or the sample must be moved synchronously with the shoot of the camera. The Microscope used was the Olympus BH2-MJLT. Using this microscope, it is possible to do observations by transmittance or reflectance of light in tissue, with magnifications of 5x, 10x, 20x, 50x and 100x. It has its own source of light which consists in a power adjustable halogen bulb (Philips CAPSUline PRO 13102).

This light has been tested to emit in all the spectral range previously mentioned. So as to obtain a hypercube from the pathology slides, a linear-movement mechanism has been employed. This mechanism is based on a Sony PlayStation 3 (PS3) BlueRay reader driver, with a movement resolution of 9 µm. This mechanism is synchronized with the capture of each pushbroom line of the camera. A full custom C++ based software has been developed to control both the camera and the mechanism movement. In order to attach the linear-movement mechanism into the microscope, a wooden flat platform has been built and replaced by the original plate of the microscope (Figure 21, right side). The slides were coupled to the PS3 driver using permanent magnets. A Graphical User Interface (GUI) has been developed to provide users an easy-to-use interface, which encapsulates the complexity of the capture system in a single button.

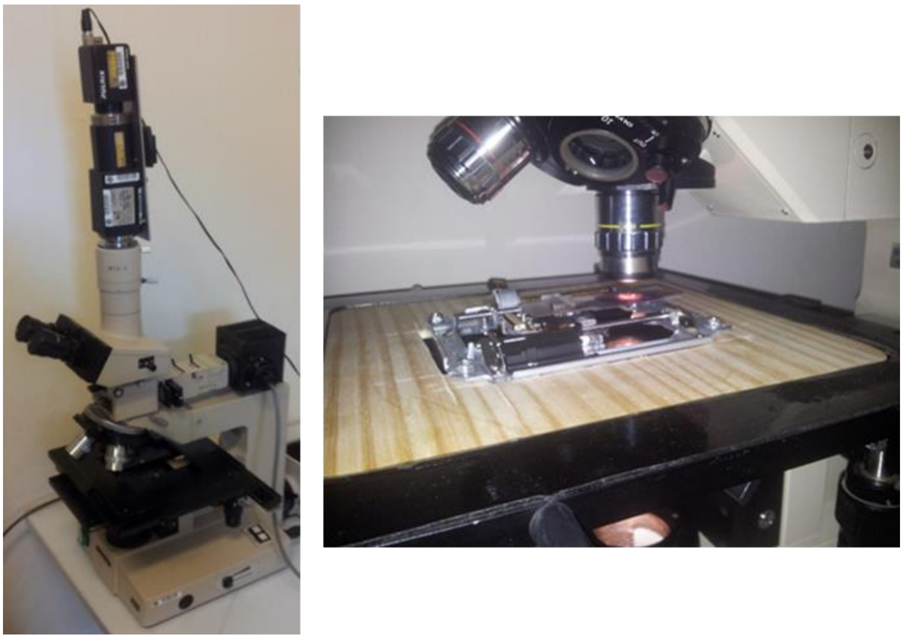

Figure 21: Microscopic hyperspectral acquisition system

The following conclusions were reached from the test of the acquisition system developed:

- When coupling the microscope with the HSI camera, the pushbroom line captured width is 4.4 µm using 5x magnification and 2.2 µm with 10x magnification. Due to the resolution of the stepper motor, which is of 9 µm, the collected hypercubes have some missing spatial information between each pushbroom lines captured.
- It has been found that the microscope heavily filters the wavelengths above 800 nm.
- The hypercubes have only been captured using the transmittance observation mode and only with 5x and 10x magnifications. The sensitivity of the HSI camera sensor does not allow making observations neither with reflectance observation technique nor using the other available lenses. This is because the power of the light source used is not bright enough to make measures in the reflection mode or with higher magnification lenses.

3.3 Hyperspectral dataset

The spectral database described in [47] consists in 83 hypercubes in each magnification, 5x and 10x. Due to the high dimensionality of data and the computational cost associated with processing this high amount of data, in this research study only 19 hypercubes have been selected (all of them captured with 5x magnification). In Figure 22 a RGB representation of certain hypercubes are shown. As previously named, tissue inside red markers have been diagnosed as tumoural, and tissue inside blue marker has been diagnosed as normal tissue.

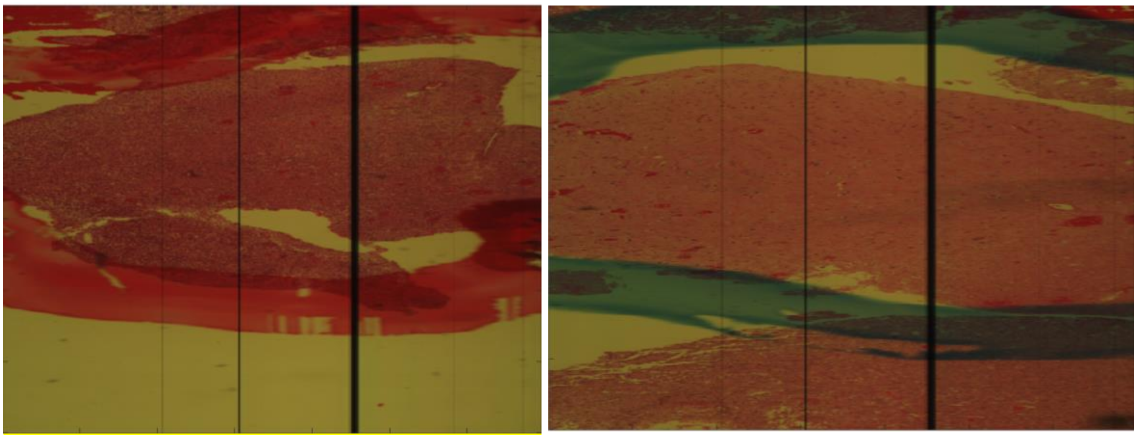

Figure 22: RGB representation of two hypercubes used in this study

As mentioned in the description of the acquisition system, not the whole spatial information can be captured by this hyperspectral camera. Due to this fact, in this study only the spectral information will be taken into account. If the full spatial information were available, we were allowed to exploit the morphological characteristics of tissue, and permitting to include the same criteria used by pathologist when they are diagnosing. Figure 23 shows a typical histological image used by pathologist to diagnose brain tumour. Compared with Figure 22, it can be seen how the histological image allow distinguishing cells, while it is not possible in the acquired hyperspectral images.

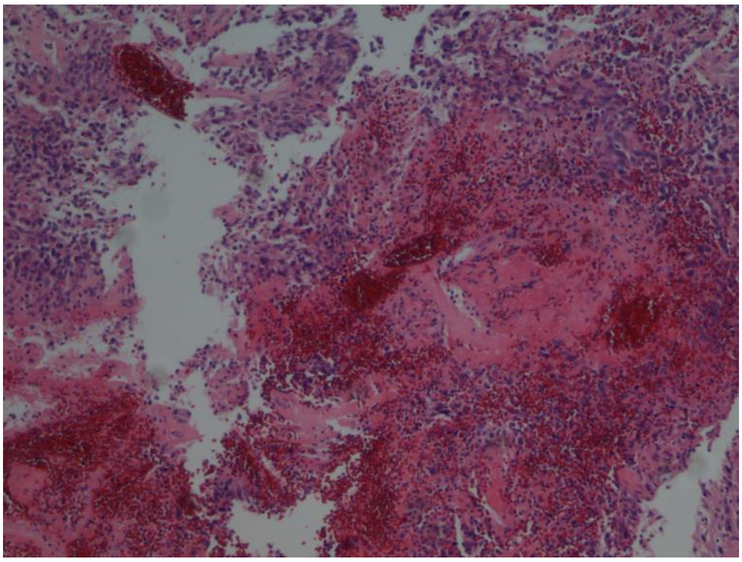

Figure 23: Histological image from brain tissue

Using this hypercubes, a region of interest (ROI) of each hypercubes have been defined in order to create a spectral dataset, and the useful spectral information have been extracted. Table 1 summarizes the spectral dataset available for each patient after defining the ROI and extracting the spectral data.

	P1	P2	P3	P4
Normal Tissue	132367	138453	90436	-
Tumour Tissue	122801	131830	122646	81067

Table 1: Spectral dataset summary

The spectral signatures for both classes and all patients are shown on Figure 24. These spectral signatures have been calculated as the mean spectra of each kind of tissue for each patient. The spectra represented using a blue line belongs to normal tissue and a red line is used to draw the spectra from tumour tissue. After the visual inspection of this spectral signatures, it can be easily noticed that there are significant differences between normal and tumour tissue. It can be observed that there are similarities between the different types of tissue among the different patients. In other words, the shape of the spectral signature of normal tissue is similar for all patients. The same trend keeps for the tumour tissue.

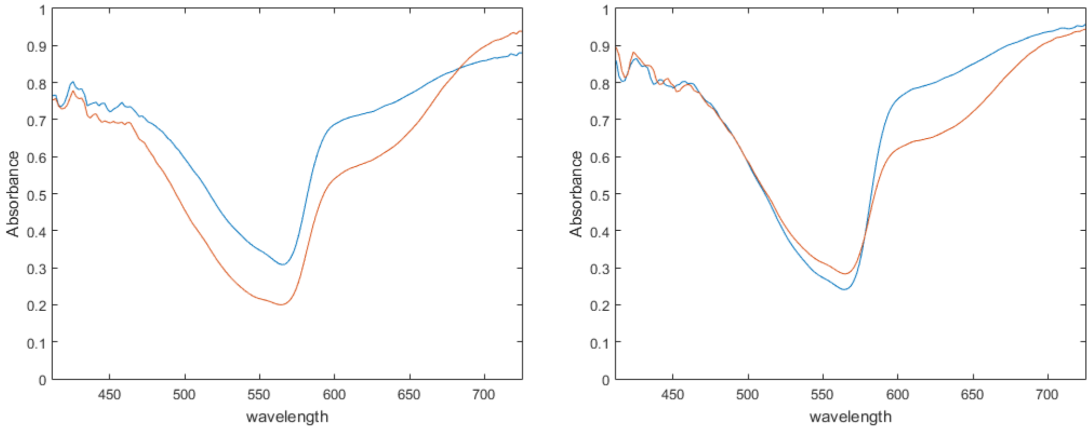

(a) Patient #1

(b) Patient #2

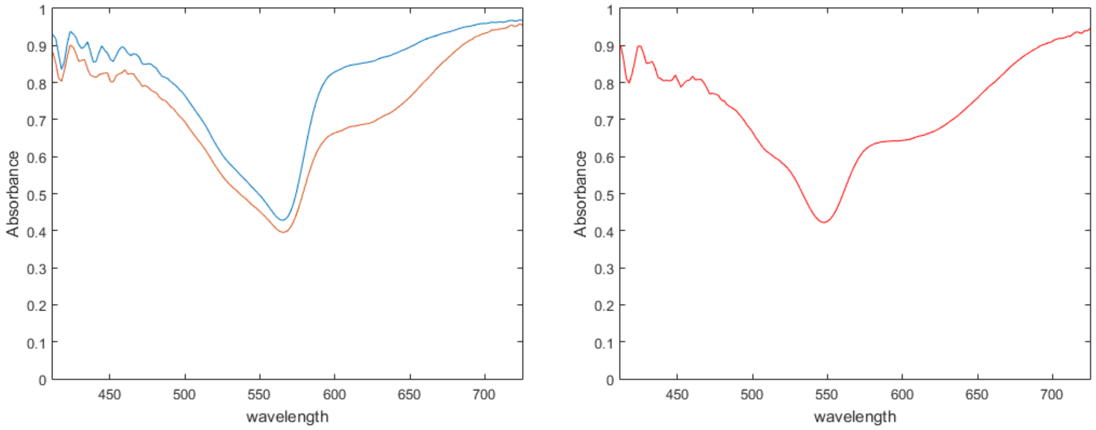

(c) Patient #3

(d) Patient #4

Figure 24: Spectral signatures extracted from the dataset

3.4 Case Study description

In order to validate supervised classification algorithms for discriminating between healthy and tumour tissue, three different case studies (CSs) have been proposed. This approaches differs in which patients are included as subject of study. Each case study can be accomplished using different pre-processing stages and different classification algorithms. These proposed scenarios are described below.

CASE STUDY 1 (CS1)

The goal of this CS is to check if the discrimination between healthy and tumour tissue can be performed using the available labelled data, and avoiding the inter-patient variability of data. In other words, this means that the datasets explored in this CS include hypercubes from pathological slides from a single patient, where both type of tissue (healthy and tumour) are present. In order to avoid the inter-patient variability of data, each patient's data is used independently for training and testing a supervised classifier.

This CS simulations will be accomplished for patient numbers' 1, 2 and 3, because data need both types of tissue to perform a supervised classification between the two types of tissue. Patient number 4 is not included in this CS because only tumour samples are available.

CASE STUDY 2 (CS2)

In CS2 all the available labelled data are merged in a unified dataset. It means that a unique database is created by joining all single patient data, so in this scenario the inter-patient variability is taken into account. In Table 2 the description of the dataset used in this CS is summarized.

	Normal Tissue	Tumour Tissue
Number of Samples	377277	442323

Table 2: CS2 dataset description

CASE STUDY 3 (CS3)

This case study is the most realistic one in a diagnosis context. In this approach, the data from one patient is used as test set of a classification algorithm, and that classifier model is built using the information from the whole rest of hyperspectral labelled data (belonging to the other patients). This case study represents the real case of a new sample arriving to the pathologist laboratory, where the classification must be performed with a classifier trained with data from previous patients. The dataset description of this CS is summarized in Table 3.

	Train Samples		Test Samples	
	Normal Tissue	Tumour Tissue	Normal Tissue	Tumour Tissue
Patient #1	254476	309956	132367	122801
Patient #2	245447	303870	138453	131830
Patient #3	254631	351887	90436	122646
Patient #4	377277	361256	-	81067

Table 3: CS3 dataset description

3.5 Processing Framework

The proposed processing framework is based on a typical supervised classification scheme. Although it has been proven that combining both the spatial and spectral features of the hyperspectral images can improve the accuracy in the predictions, in this research work only the spectral characteristics of the data are taken into account. This way, the inputs of the classifier are the measured spectral signature from healthy and tumour pixels. The first stage consists on a preprocessing chain that aims to compensate the effects produced by both the environmental conditions and the system response of the capture system during the acquisition of the hypercubes. Then, a supervised classification is performed using three different classification methods. Finally, the performance of the classifiers is evaluated using standard metrics for assessing a classifier performance. This workflow is represented in Figure 25. This section provides the details of each stage of this workflow in this research work.

Figure 25: Processing framework used in this research work

3.5.1 Preprocessing

The preprocessing stage proposed in this research work is shown in Figure 26. First, due to the high dimensionality of the hypercubes, that deeply slow the processing of data, a manual Region of Interest (ROI) selection is applied. In this procedure, the selection of the area of interest has been carefully performed taking a ROI that is a middle solution between selecting a large area (which can raise a high computational cost) and choosing enough relevant data inside each scene. In Figure 27, a synthetic RGB representation of the full hypercube and the defined ROI is presented.

Figure 26: Preprocessing chain

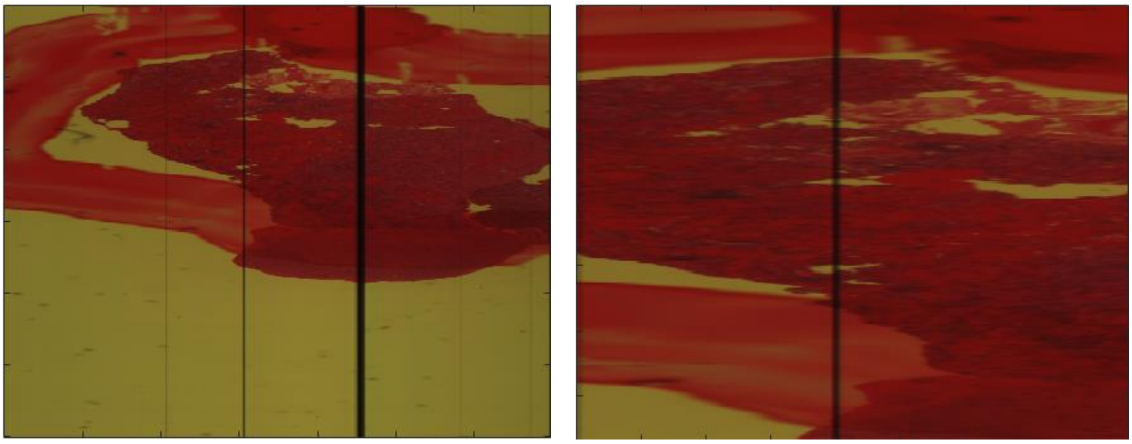

Figure 27: Original cube size and ROI selection

The second stage of the preprocessing chain is related to the calibration of the image. Through the calibration the acquired image is converted from radiance observation to absorbance. The absorbance is used calculated by taking the ratio between the sample image with respect to a reference image. The reference material provides a measure of the instrument response function from the resultant optical density image set [48]. Figure 28.a presents the raw data acquired by the hyperspectral camera. Figure 28.b shows the reference spectra, that has been acquired as the light that is captured by the camera after passing through an empty pathological slide. Finally the calibrated spectra, once Equation 1 have been applied is shown on Figure 28.c.

$$I_{abs} = -\log\frac{I_{raw}}{I_{ref}} \qquad \text{Equation (1)}$$

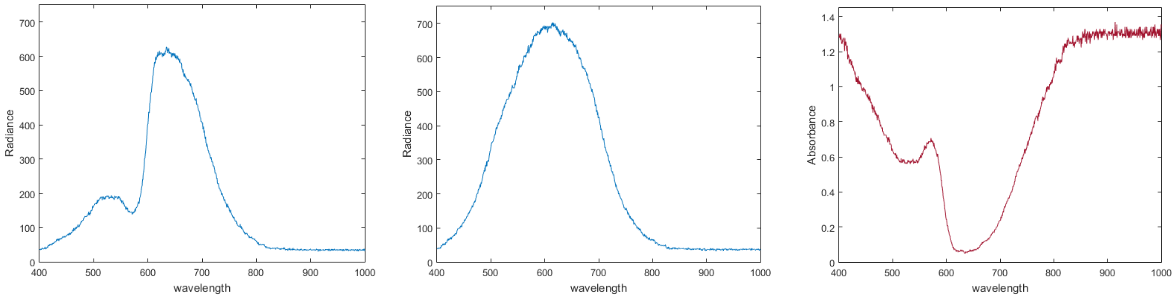

(a) (b) (c)

Figure 28: (a) Raw spectra (b) Reference Spectra (c) Calibrated spectra

The next step in the preprocessing chain is performing a band reduction of the hypercube. The motivation is performed in two ways. In the one hand, there are bands that do not carry any information. In the reference spectra on Figure 28 it can be seen that the measured intensity is almost zero for the extreme wavelengths. This information is cleared in order to eliminate the meaningless information. The selected operating bandwidth can be observed in Figure 29.a, and covers the spectral range from 410 nm to 750 nm. On the other hand, the measured spectrum has high redundancy between contiguous bands. This fact is caused due to the high resolution of the camera sensor related with the diffraction capability of the optical grating. For the spectral system employed in this work, the spectral resolution is 3nm and the captured spectral bands are 1040. This means that the contiguous bands has been sampled each 0.6nm approximately, acquiring redundant information due to the impossibility of the optical system to sample the spectrum with that spectral resolution. In order to avoid this redundancy, the spectral bands are averaging in order to reduce the both the dimensionality and the redundant information [49]. The spectra after applying the band average can be observed in Figure 29.b, it can be seen that the shape does not change compared with the same spectra with 1040 spectral bands (Figure 28.c).

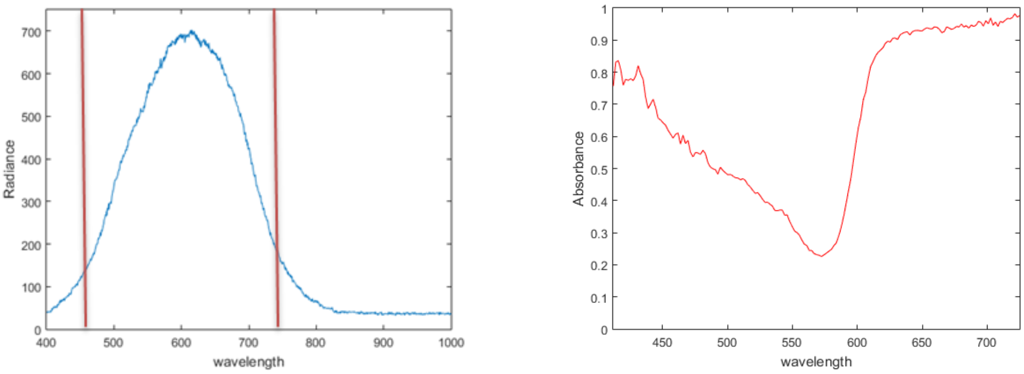

(a) (b)

Figure 29: (a) Operating bandwidth (b) Spectra after band reduction

The next step of the proposed preprocessing chain consists in removing the spatially aberrated pixels caused by the presence of bad columns in the CCD used by the hyperspectral system. Bad columns are artefacts that appear in the read out progress in CCD cameras, and cause that several lines in the acquired image are not valid. In order to remove these artefacts from the hypercubes, a mask containing the location of the bad columns in the hypercube is used to avoid the pixels affected by the bad columns defect.

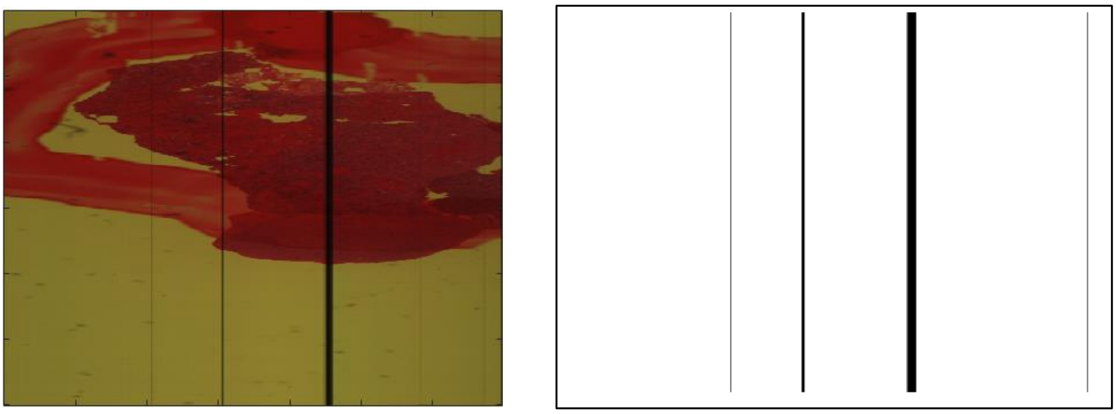

(a) (b)

Figure 30: (a) Hypercube affected by bad columns (b) Mask showing the location of bad columns

Finally, in order to process uniquely the useful information, a way for discriminating between pixels that belong to the microscope light has been proposed. Due to the white colour of the measured light, binarization is performed to a RGB image extracted from the hypercube. After manually selecting a suitable threshold, it is possible to locate the microscope light in order to avoid processing that meaningless pixels (Figure 31).

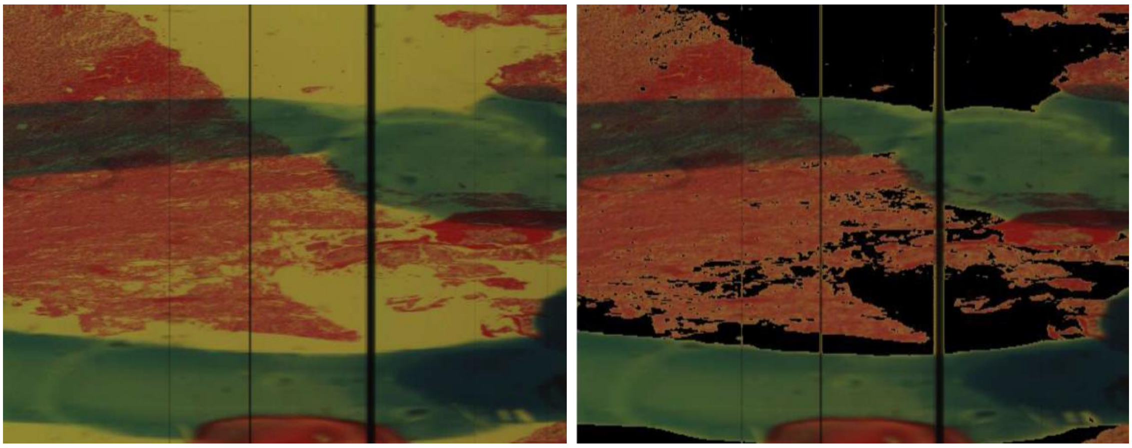

(a) (b)

Figure 31: (a) Synthetic RGB from a hypercube (b) RGB image where microscope light has been removed

3.5.2 *Model Evaluation*

For classification problems, the classifier performance is usually measured as the error rate of the classifier. The classifier predicts the class for each instance in the dataset: if the class of the instance is correctly predicted it is counted as a success. Controversially, if the predicted label is not the same as the label of the instance that have been classified it is a classification error. The error rate is just the proportion of errors made over a whole set of instances, and it measures the overall performance of a classifier.

The error rate measured over the training set is not likely to be a good indicator of future performance, because the classifier has been trained using the same training data, so the error estimation based on the training data will be optimistic. To predict the performance of a classifier over new data, it is necessary to assess its error rate on a dataset that played no part in the formation of the classifier. This independent dataset consisting in previously unseen data is called the test set.

If the number of instances in the dataset is high, there is no problem. In such case it is possible to split the dataset into two disjoint sets with a large number of instances. Then, one of these subsets can be used to train the classifier and the other can be used to measure its performance.

The problem appears when the available data is limited, and this is the typical situation in most of practical machine learning scenarios. In such situations, the amount of data that can be used for train and evaluate the performance of the classifier are limited. Generally, the larger training sample the better classifier, and the larger test samples, the more accurate the error estimate. So a trade-off arises: to find a good classifier it is advisable to use as much data for training, and to obtain a good error estimate it is necessary to use as much of it as possible for testing.

In the Machine Learning literature, it is possible to find several strategies to tackle this problem, in this document the hold out and the cross-validation methods will be employed.

HOLD OUT:

This method for assessing the performance of a classifier simply consists on selecting a certain amount of data for measuring the model performance and reserving the rest of instances on the training set for building the classifier. In practical terms, it is common to hold out one third of the data for testing and the remaining two-thirds for training [49].

This method has a lack: it is possible that neither the sample used for training nor testing or even both might be not representative. At least, the hold out procedure must guarantee that all classes are represented both in the training set and in the test set. This procedure is called stratification. A more general way to mitigate any bias caused by the particular sample chosen for holding out is to repeat the whole process, training and testing, several times with different random samples. The error rates of the different iterations are averaged to yield an overall error rate. This method is called repeated hold out error rate estimation [50].

CROSS VALIDATION:

In the k-fold cross-validation method the whole dataset is partitioned into k disjoint folds. As occurs in the hold out method, it is advisable that each fold has the same class proportion. The basis of this method consist in using *k-1* folds for training a classifier and the remaining for assessing its performance. This procedure is repeated *k* times varying the test set in each iteration until all folds have been used to evaluate the model performance. Finally, the model performance is calculated as the average performance of the *k* iterations. Figure 32 shows a graphical representation of this method with *k* = 10, where the fold used to evaluate the model in each iteration is highlighted in red colour.

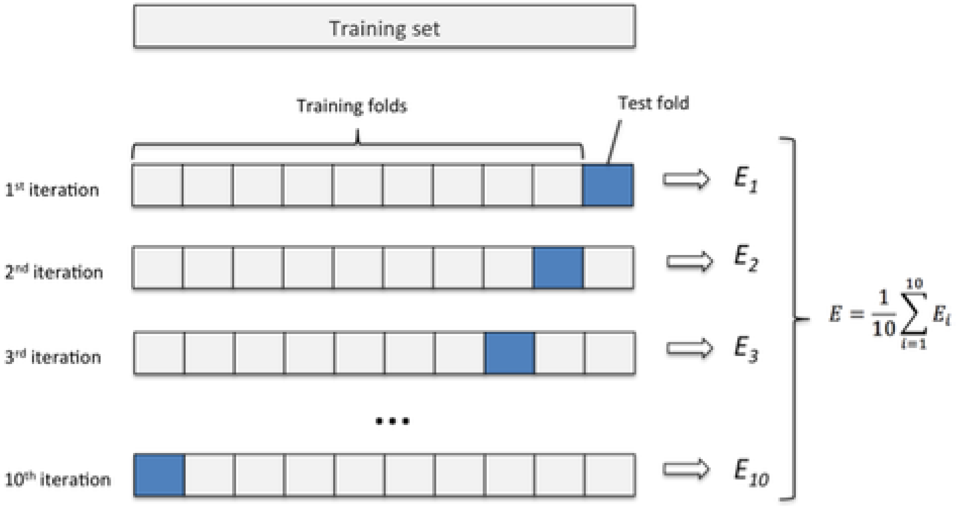

Figure 32: K-fold cross-validation example

Extensive test on numerous different datasets, with different learning techniques have shown that k = 10 fold is the right number of fold to get the best estimate of error, and tenfold cross validation has become the standard method in practical terms. Nevertheless, a single tenfold cross-validation might not be enough to get a reliable error estimate. When seeking an accurate error estimation, it is a standard procedure to repeat the tenfold cross-validation several times and average the results [50].

In this research study, 10-fold cross validation will be used as model validation scheme for CS1 and CS2. In CS3 is not possible to apply cross validation, so the model will be evaluated using hold-out validation, where the test set correspond to the spectral samples from one patient, and the classifier is trained using the samples from the other patients.

3.5.3 Selected classification algorithms

An extensive literature is available on pixel-wise classification of hyperspectral images, where each pixel is assigned to one of the classes based exclusively on its spectral signature. For this purpose, methods based on decision trees, neural networks and kernel-based methods has been widely used. These algorithms have to face with two main problems: the high dimensionality of data and a limited size of sample data. The selected algorithms for this research work are Support Vector Machine (SVM), Artificial Neural Networks (ANN) and Random Forest (RF).

SVM is a kernel-based supervised algorithm that has been extensively used in the classification of hyperspectral images. In the bibliography, it has been proved that SVM provides a good performance for classifying hyperspectral data when a limited number of training samples are available [51]. Due to its strong theoretical foundation, good generalization capabilities, low sensitivity to the curse of dimensionality, and ability to find global classification solutions, SVM is usually preferred by many researchers over other classification paradigms for classifying hyperspectral images [15]. In this research work LIBSVM [52], integrated software for support vector classification, has been employed.

Recent remote sensing literature has shown that SVM methods generally outperform traditional statistical and artificial neural networks methods in classification problems involving hyperspectral images. Nevertheless, neural networks has been also successfully used in the classification of hyperspectral images [51][53]. In the hyperspectral medical field, some studies has applied neural networks as classifier [54][55]. The neural network used in this research work is a feed forward Multilayer Perceptron (MLP) network, trained using a backpropagation algorithm. The MATLAB Neural Network Toolbox has been chosen to test the quality of these algorithms to the available data.

The other algorithm used in this supervised classification approach is Random Forest. Random Forest is an ensemble classification algorithm, which constructs a set of classifiers and then classify new data by taking a vote of their predictions [56]. Some studies have shown that these ensemble methods can provide a classification result as accurate as other traditional classifiers, like neural networks [57]. Although these algorithms have not been used in the classification of medical hyperspectral images, in this work both algorithms will be used as pixel-wise classifiers. In order to test this supervised ensemble algorithms, the MATLAB Machine Learning ToolBox has been employed.

3.5.4 Evaluation Metrics

Metrics chosen for estimating the classifier performance in this study are sensitivity, specificity and overall accuracy. This metrics summarizes the information supplied by a confusion matrix, but due to the large number of simulations that are being performed (there are several simulations from each case study, and each case study is performed using different classification algorithms), the confusion matrices are not provided. The evaluation metrics employed in this research work are sensitivity, specificity and overall accuracy. Before providing the definitions of these supervised classification metrics, some terms must be defined:

- **True Positive (TP):** Correctly detected conditions. In other words, the result of the test is positive and the actual value of the classification is positive.
- **False Positive (FP):** Incorrectly detected conditions. The result of the test is negative and the actual value of the classification is positive.
- **True Negative (TN):** Correctly rejected conditions. The result of the test is negative and the actual value of the classification is negative.
- **False Negative (FN):** Incorrectly rejected conditions. The result of the test is positive and the actual value of the classification is negative.

The standard classification metrics employed in this study can be summarized as follows:

Sensitivity: Is the proportion of actual positives that are correctly identified as positives by the classifier. It is computed as follows:

$$Sensitivity = \frac{TP}{TP + FN} \qquad \text{Equation (2)}$$

Specificity: Is the proportion of the actual negatives that the classifier successfully tests negative for it. It is expressed as follows:

$$Specificity = \frac{TN}{TN + FP} \qquad \text{Equation (3)}$$

Overall Accuracy: Refers to the ability of the model to correctly predict the class label of new or previously unseen data. Equation 4 shows formula of the overall accuracy metric.

$$Overall\ Accuracy = \frac{TP + TN}{TP + FP + TN + FN} \qquad \text{Equation (4)}$$

3.6 Summary

In this chapter, the biological samples employed in this study have been presented, providing both the medical information and describing how the samples have been captured using a hyperspectral acquisition system. Then, the methodology followed in this research work has been described. First, some different experiments have been proposed. These experiments differ in how the models are built, taking or not into account the inter-patient variability of data. Finally, the processing framework used in this research work is presented. This processing framework includes a preprocessing stage, three types of supervised classifiers and different model evaluation techniques.

Chapter 4: Results

This chapter presents the results achieved when applying the supervised classification framework described on Chapter 3. These results consist in the performance estimation of each classifier in each Case Study. Also the computational cost of each classifier is shown as a measured of the time required to train and evaluate the performance of each classifier.

For the SVM classifier, two different set ups have been tested: a linear kernel classifier and a Gaussian (Radial Basis Function, RBF) kernel. Regarding the topology of the neural network, several neural networks architectures varying the number of hidden layers, the number of neurons inside this layers and the activation function selected for each layer have been tested. The experimental results shown that the best performance is obtained using a multilayer neural network with a single hidden layer composed by 16 neurons, using a logistic activation function for this layer. A hyperbolic tangent sigmoid activation function has been selected for the output layer. Finally, an ensemble of 50 different classification trees composes the Random Forest configuration.

4.1 Case Study 1

As named in Chapter 3, CS1 consists on classifying data that uniquely belongs to a single patient. For this reason, and due to the absence of normal tissue for patient number 4, only patients 1, 2 and 3 are included in this experiment. The estimation of the model performance has been obtained using 10-fold cross-validation.

4.1.1 Support Vector Machines

The results for SVM using both kernels, linear and Gaussian, are shown in Table 4 and Table 5 respectively. It can be seen that the results achieved in this experiment can perfectly discriminate between normal and tumour tissue with high sensitivity and specificity. Comparing the results of each classifier's configuration it can be observed that using the linear kernel it is possible to achieve better results than the Gaussian kernel with a lower computational cost.

Patient	Overall Accuracy	Sensitivity	Specificity	Time (1 fold)	Time (CV)
P1	99.04%	99.29%	98.76%	26.06 min	4.34 hours
P2	98.48%	98.75%	98.20%	32.99 min	5.49 hours
P3	99.67%	99.87%	99.52%	5.42 min	0.90 hours

Table 4: Classification results, CS1 and linear SVM

Patient	Overall Accuracy	Sensitivity	Specificity	Time (1 fold)	Time (CV)
P1	97.34%	97.56%	97.10%	91.54 min	15.25 hours
P2	97.18%	97.47%	96.89%	93.25 min	15.54 hours
P3	98.78%	99.81%	98.06%	31.92 min	5.32 hours

Table 5: Classification results, CS1 and RBF SVM

4.1.2 *Artificial Neural Network*

The results obtained using ANN are shown on Table 6. These results outperform 99% of overall accuracy for every patient. In terms of specificity and sensitivity these results show a good discrimination rate between the different classes, being the sensitivity and specificity values also higher than 99% in all the cases. Regarding the computational cost, ANN show a much lower computational cost compared with the SVM approaches for this CS.

Patient	Overall Accuracy	Sensitivity	Specificity	Time (1 fold)	Time (CV)
P1	99.17%	99.13%	99.20%	3.59 min	0.59 hours
P2	99.95%	99.96%	99.94%	3.75 min	0.62 hours
P3	99.82%	99.90%	99.76%	3.06 min	0.51 hours

Table 6: Classification results, CS1 and Neural Networks

4.1.3 *Random Forests*

Using Random Forests, it is also possible to accurately differentiate between normal and tumour tissue by uniquely attending to the spectral signature of each type of tissue. Table 7 shows the results for this classifier, where it can be observed that the worst classification have been obtained for patient number 1. This classifier show the lowest computational cost compared to the others.

Patient	Overall Accuracy	Sensitivity	Specificity	Time (1 fold)	Time (CV)
P1	98.77%	98.67%	98.88%	2.66 min	0.44 hours
P2	99.66%	99.73%	99.58%	2.54 min	0.42 hours
P3	99.36%	99.77%	99.07%	2.13 min	0.35 hours

Table 7: Classification results, CS1 and Random Forests

The results achieved in the CS1 scenario shows that all the classification algorithms can obtain great classification results. The worst results in terms of overall accuracy is higher than 98% of success, and the values of sensitivity and specificity in this case hold higher too. As far as computational cost is concerned, it can be seen that ANN and RF can overwhelm the classification task more efficiently.

The graphical representation shown Figure 33 is a useful way to display multivariate data. It consists on a radial graph; where the edged represent a classifier and each point represent a classification result. From this representation it is possible to extract some information. Regarding to the classifiers, it can be seen that ANN obtain the most accurate results for all the evaluation metrics. Random Forests also provides accurate classification results, outperforming both SVM configurations. On the other hand, regarding to the results obtained for each patient, patient number 3 show better prediction than the others, specifically this patient show high sensitivity values for all the classifiers. The other patients show a similar trend, obtaining competitive predictions for all the classifiers.

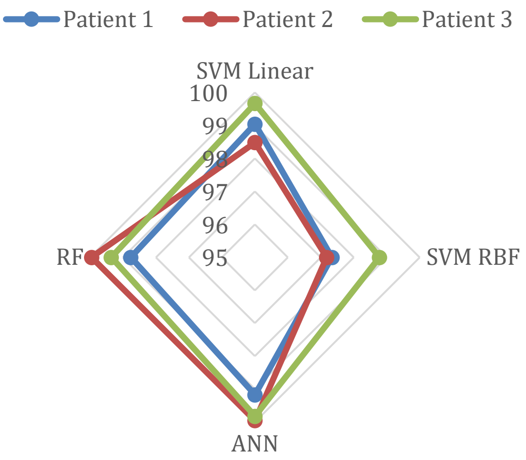

(a)Overall Accuracy

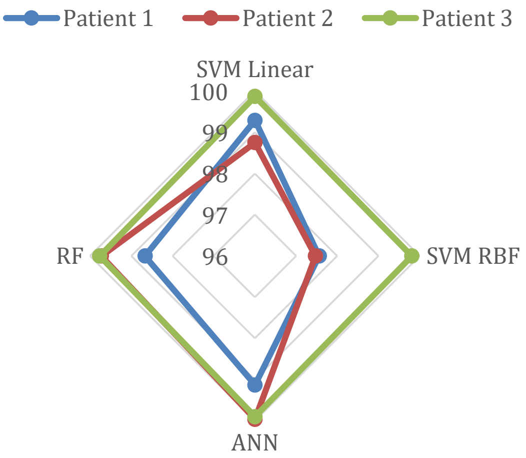

(b) Sensitivity

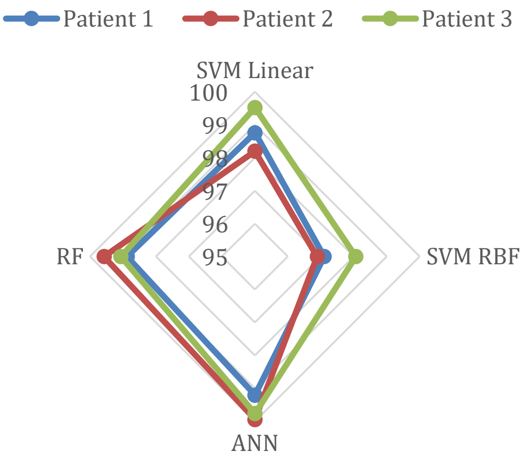

(c) Specificity

Figure 33: Graphical representation of results – CS1

4.2 Case Study 2

This CS aims to introduce some inter-patient variability in the classification routine. This is done by merging all available data from all patients in a single dataset. The model evaluation has been also accomplished through 10-fold cross-validation. The results achieved with all the classifiers for this case study are shown on Table 8. Although the discrimination rate in all supervised classifiers present good discrimination capabilities between normal and tumour tissue (higher than 90% in terms of overall accuracy, sensitivity and specificity), the results have worsened compared to the ones obtained in CS1. Following the same trend as in CS1, ANN provides the best classification results. It can be also observed that the results achieved using SVM are the weakness ones.

Classifier	Overall Accuracy	Sensitivity	Specificity	Time (1 fold)	Time (CV)
SVM Linear	94.46%	95.15%	93.66%	712.20 min	118.70 hours
SVM RBF	92.78%	94.55%	90.83%	1168.40 min	194.73 hours
RF	97.91%	98.06%	97.75%	12.42 min	2.07 hours
ANN	98.20%	98.72%	97.61%	11.24 min	1.87 hours

Table 8: Classification results, CS2

Talking about computational cost, it has been heavily increased compared with the ones obtained in CS1. This is due to the high amount of data that compose the dataset (more than 800,000 samples). In this CS, the computational time required by SVM is much greater than the one required for both ANN and RF. The time spent by ANN and RF for training the classifier and evaluating its performance can be measured in a few hours, meanwhile the time required by both SVM variants must be measured in days. For these reasons, ANN and RF provide more competitive predictions with a significantly lower computational cost.

A radial graph is used again to obtain a graphical representation of the results. In this case, due to the presence of a unique simulation, all the evaluation metrics are plotted simultaneously. Figure 34 indicates that the best classification results are reached when using ANN and RF. Again the worst classification results have been obtained with SVM and Gaussian kernel. It must be observed that the values of specificity and sensitivity are balanced, so the classifiers are capable to distinguish between both types of tissue with a similar accuracy.

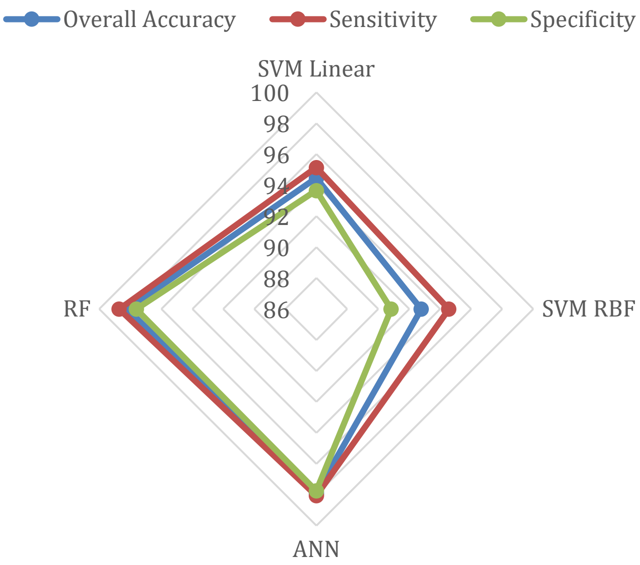

Figure 34: Graphical representation of results – CS2

4.3 Case Study 3

This experiment setup reproduces a practical situation where a new patient arrives and the prediction of the disease is based on the information from the previous patients. In this scenario, the model evaluation is performed following a hold-out method, where the samples from previous patients are used as training set and data from the new patients is used to evaluate the model performance. Patient number 4 only has samples from tumoral tissue, so the measure of the specificity does not make sense because there is not possible to have any false positive neither true negative. In this case the overall accuracy and the sensitivity are the same.

4.3.1 Support Vector Machines

Table 9 and Table 10 show the results obtained using SVM. It can be seen how the classification results are not as accurate as in the others case studies. Linear kernel shows poor classification results, specifically it is shown in the patient number 4. The most accurate results with this kernel is given for patient 1, achieving an 81.85% of overall accuracy. Looking at the classification results obtained for the Gaussian kernel, it has been possible to accurately classify tissue from patient number 4, achieving a 94.50% of overall accuracy.

Patient	Overall Accuracy	Sensitivity	Specificity	Time
P1	81.85%	86.94%	77.57%	6.81 hours
P2	64.64%	75.96%	59.66%	3.65 hours
P3	68.92%	59.33%	83.87%	6.52 hours
P4	10.74%	10.74%	-	11.93 hours

Table 9: Classification results, CS3 linear SVM

Patient	Overall Accuracy	Sensitivity	Specificity	Time
P1	73.86%	79.19%	69.65%	821.35 min
P2	61.19%	68.46%	57.51%	483.07 min
P3	58.44%	50.58%	83.52%	817.09 min
P4	94.50%	94.50%	-	1164 min

Table 10: Classification results, CS3 RBF SVM

4.3.2 Artificial Neural Network

The results obtained using Artificial Neural Networks, presented in Table 11, are not accurate at all. For patient 4 the predictions are really precise, achieving a 99.20% of overall accuracy, but the results obtained for the other patients are not useful. Regarding the computational cost, it is more efficient compared with the two SVM variants.

Patient	Overall Accuracy	Sensitivity	Specificity	Time
P1	48.15%	50.03%	46.19%	9.70 min
P2	47.26%	47.80%	46.99%	9.48 min
P3	33.02%	15.23%	42.72%	10.47 min
P4	99.20%	99.20%	-	12.95 min

Table 11: Classification results, CS3 and Neural Networks

4.3.3 Random Forests

Table 12 shows the evaluation metrics obtained for Random Forests. The trend is similar to the ones achieved using Neural Networks: all the results are really inaccurate, excepting the ones reached for patient number 4, where an 88% of overall accuracy was obtained.

Patient	Overall Accuracy	Sensitivity	Specificity	Time (1 fold)
P1	47.75%	49.60%	46.13%	6.66 min
P2	38.50%	39.53%	37.51%	6.16 min
P3	41.29%	39.27%	47.62%	6.67 min
P4	88.04%	88.40%	-	9.26 min

Table 12: Classification results, CS3 and Random Forests

In Figure 35, a radial graph represents the classification results for this scenario. It can be observed that the most accurate results are obtained when classifying patient number 4. These results are above 88% overall accuracy using all classifiers except SVM with linear kernel. Regarding the other patients, the classification results are very inaccurate when ANN and RF are employed (worse than a random assign of classes). SVM provides better classification results compared to the others, and also show some promising results for patient 1. These results are not as accurate as the obtained in the others CS, but they show that it is possible to correctly classify data from other patient. These results are 88% and 73% of overall accuracy for the SVM linear and SVM RBF respectively.

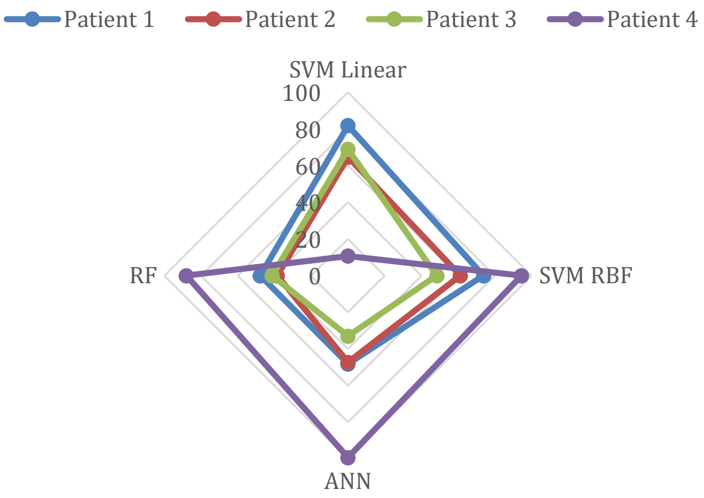

(a)Overall Accuracy

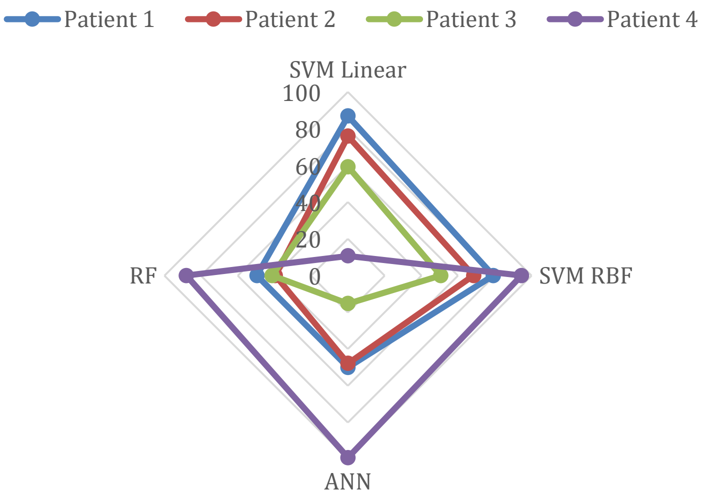

(b) Sensitivity

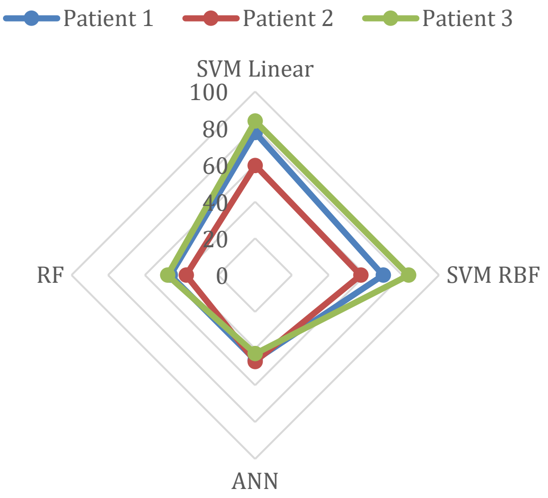

(c) Specificity

Figure 35: Graphical representation of results – CS3

Finally, the results of this CS3 are briefly compared. It can be easily seen that the classification accuracy has decreased compared to the achieved in the other case studies. It can be also observed that the sensitivity and specificity values are not balanced, as occurs in the others case studies. In this CS3 only the samples from patient number 4 have been classified accurately (except using SVM with linear kernel).

4.4 Summary

This chapter presents the classification results obtained in this research work. The performance of three different supervised classifiers have been evaluated over three different scenarios, where the inter-patient variability was or not taken into account. These results are promising in CS1 and CS2, showing that it is possible to distinguish between normal and tumour tissue attending only to the spectral signature. In CS3 the results are not as accurate, possibly due to the low number of patients involved in this study.

Chapter 5: Conclusions

The main goal of this Master's Thesis, propose and validate several classification models and use data mining techniques in order to obtain an automatic diagnostic tool for medical hyperspectral imaging, have been successfully achieved. Also an exhaustive documentation about the medical hyperspectral images have been acquired, finding new ways to threat the same problem with different points of view (for example, following a strategy similar to the one followed by the Norwegian research group analysed in Chapter 2).

As far as classification results is concerned, it has been shown in Chapter 4 that competitive results in the discrimination between normal and tumour tissue are obtained in CS1 and CS2 whatever classifier is employed. This trend does not keep in CS3, where only in certain specific situations (patient number 4 with Gaussian kernel SVM and with ANN) accurate predictions are obtained. The low number of patients involved in this study possibly causes the inaccurate results reached in CS3. Using only four patients, the classifier is built uniquely using the information from three patients. Moreover, due to the fact that patient number 4 only provides samples for tumour tissue; patients 1, 2 and 3 are trained using healthy tissue information from only two patients. For these reasons, it is possible that the classifiers have not enough information to build a model with high generalization, and the model is highly biased by the patients. In future works the number of patients must be increased in order to avoid this fact.

Regarding the supervised classifiers used in this study, in CS1 and CS2 the better classification results are obtained using ANN and RF. These algorithms have also shown the lower computational cost compared with SVM. In CS3 there is no tendency, some algorithm works correctly with certain patients. The ongoing work in this field can be based on introducing additional processing techniques, like feature selection and extraction. This has not been accomplished in this Master Thesis due to its temporal constraints and the high simulation time required for each simulation.

It has been proven in the literature regarding hyperspectral image classification that combining both the spatial and spectral features extracted from hyperspectral data enhance the prediction accuracy. Specifically, in this context the inclusion of the spatial features can be advantageous, because the gold standard of cancer diagnoses is based on the morphological analysis of pathological slides. Nevertheless, the data employed in this study do not have enough spatial resolution to exploit the morphological information of data.

Summing up, although more efforts must be put in developing an automatic diagnostic tool for pathological slides, hyperspectral imaging has been presented as a suitable tool for handling this problem. While a more exhaustive study must be carried out, including more patients, hyperspectral images with higher spectral resolution and more sophisticated classification schemes, this study presents promising results in discriminating between normal and tumour tissue in pathological slides. This kind of tools can help pathologist to analyse the slides without spending a long time for the examination of each sample.

Bibliography

[1] Solomon, J., & Rock, B. (1985). Imaging spectrometry for earth remote sensing. Science, 228(4704), 1147-1152.

[2] Richards, J. A., & Richards, J. A. (1999). *Remote sensing digital image analysis* (Vol. 3). Berlin et al.: Springer.

[3] Underwood, E., Ustin, S., & DiPietro, D. (2003). Mapping nonnative plants using hyperspectral imagery. *Remote Sensing of Environment*, *86*(2), 150-161.

[4] Wu, D., & Sun, D. W. (2013). Advanced applications of hyperspectral imaging technology for food quality and safety analysis and assessment: A review—Part I: Fundamentals. *Innovative Food Science & Emerging Technologies*, *19*, 1-14.

[5] Wu, D., & Sun, D. W. (2013). Advanced applications of hyperspectral imaging technology for food quality and safety analysis and assessment: a review—part II: applications. *Innovative Food Science & Emerging Technologies*, *19*, 15-28.

[6] Li, J., Rao, X., & Ying, Y. (2011). Detection of common defects on oranges using hyperspectral reflectance imaging. *Computers and electronics in agriculture*, *78*(1), 38-48.Ciurczak, E. W., & Igne, B. (2014). *Pharmaceutical and medical applications of near-infrared spectroscopy*. CRC Press.

[7] Yuen, P. W., & Richardson, M. (2010). An introduction to hyperspectral imaging and its application for security, surveillance and target acquisition. The Imaging Science Journal, 58(5), 241-253.

[8] Montembeault, Y., Lagueux, P., Farley, V., Villemaire, A., & Gross, K. C. (2010, June). Hyper-Cam: Hyperspectral IR imaging applications in defence innovative research. In *2010 2nd Workshop on Hyperspectral Image and Signal Processing: Evolution in Remote Sensing* (pp. 1-4). IEEE.

[9] Plaza, A., Benediktsson, J. A., Boardman, J. W., Brazile, J., Bruzzone, L., Camps-Valls, G., ... & Marconcini, M. (2009). Recent advances in techniques for hyperspectral image processing. Remote sensing of environment, 113, S110-S122.

[10] Borghys, D., Kåsen, I., Achard, V., & Perneel, C. (2012). Hyperspectral anomaly detection: comparative evaluation in scenes with diverse complexity. Journal of Electrical and Computer Engineering, 2012, 5.

[11] Manolakis, D., Marden, D., & Shaw, G. A. (2003). Hyperspectral image processing for automatic target detection applications. Lincoln Laboratory Journal, 14(1), 79-116.

[12] Bioucas-Dias, J. M., Plaza, A., Dobigeon, N., Parente, M., Du, Q., Gader, P., & Chanussot, J. (2012). Hyperspectral unmixing overview: Geometrical, statistical, and sparse regression-based approaches. *IEEE Journal of Selected Topics in Applied Earth Observations and Remote Sensing*, *5*(2), 354-379.

[13] Santos Falcón, L. (2014). Hyperspectral image compression onboard next-generation satellites: implementation solutions on GPU and FPGAs.

[14] Huang, T. M., Kecman, V., & Kopriva, I. (2006). Kernel based algorithms for mining huge data sets (Vol. 1). Heidelberg: Springer.

[15] Li, Q., He, X., Wang, Y., Liu, H., Xu, D., & Guo, F. (2013). Review of spectral imaging technology in biomedical engineering: achievements and challenges. Journal of biomedical optics, 18(10), 100901-100901.

[16] Lu, Guolan, and Baowei Fei. "Medical hyperspectral imaging: a review." Journal of biomedical optics 19.1 (2014): 010901-010901.

[17] Akbari, H., Kosugi, Y., Kojima, K., & Tanaka, N. (2009, September). Blood vessel detection and artery-vein differentiation using hyperspectral imaging. In*2009 Annual International Conference of the IEEE Engineering in Medicine and Biology Society* (pp. 1461-1464). IEEE.

[18] Akbari, H., Kosugi, Y., Kojima, K., & Tanaka, N. (2010). Detection and analysis of the intestinal ischemia using visible and invisible hyperspectral imaging.*IEEE Transactions on*

Biomedical Engineering, *57*(8), 2011-2017.

[19] Akbari, H., Uto, K., Kosugi, Y., Kojima, K., & Tanaka, N. (2011). Cancer detection using infrared hyperspectral imaging. Cancer science, 102(4), 852-857.doi: 10.1109/TBME.2010.2049110

[20] Akbari, H., Halig, L. V., Zhang, H., Wang, D., Chen, Z. G., & Fei, B. (2012, March). Detection of cancer metastasis using a novel macroscopic hyperspectral method. In SPIE Medical Imaging (pp. 831711-831711). International Society for Optics and Photonics.

[21] Akbari, H., Halig, L. V., Schuster, D. M., Osunkoya, A., Master, V., Nieh, P. T., ... & Fei, B. (2012). Hyperspectral imaging and quantitative analysis for prostate cancer detection. Journal of biomedical optics, 17(7), 0760051-07600510.

[22] Lu, G., Halig, L., Wang, D., Chen, Z. G., & Fei, B. (2014, March). Spectral-spatial classification using tensor modeling for cancer detection with hyperspectral imaging. In SPIE Medical Imaging (pp. 903413-903413). International Society for Optics and Photonics.

[23] Lu, G., Halig, L., Wang, D., Chen, Z. G., & Fei, B. (2014, March). Hyperspectral imaging for cancer surgical margin delineation: registration of hyperspectral and histological images. In SPIE Medical Imaging (pp. 90360S-90360S). International Society for Optics and Photonics.

[24] Lu, G., Qin, X., Wang, D., Chen, Z. G., & Fei, B. (2015, March). Quantitative wavelength analysis and image classification for intraoperative cancer diagnosis with hyperspectral imaging. In SPIE Medical Imaging (pp. 94151B-94151B). International Society for Optics and Photonics.

[25] Lu, G., Wang, D., Qin, X., Halig, L., Muller, S., Zhang, H., ... & Fei, B. (2015). Framework for hyperspectral image processing and quantification for cancer detection during animal tumor surgery. Journal of biomedical optics, 20(12), 126012-126012.

[26] Pike, R., Patton, S. K., Lu, G., Halig, L. V., Wang, D., Chen, Z. G., & Fei, B. (2014, March). A minimum spanning forest based hyperspectral image classification method for cancerous tissue detection. In *SPIE Medical Imaging* (pp. 90341W-90341W). International Society for Optics and Photonics.

[27] Lu, G., Qin, X., Wang, D., Chen, Z. G., & Fei, B. (2015, March). Estimation of tissue optical parameters with hyperspectral imaging and spectral unmixing. In *SPIE Medical Imaging* (pp. 94170Q-94170Q). International Society for Optics and Photonics.

[28] SEMEOTICONS FP7 Collaborative Project No. 611516. Retrieved August 19, 2016, from http://www.iacobus-fp7.eu/

[29] IACOBUS FP7 Collaborative Project No. 305760. Retrieved August 19, 2016, from http://www.semeoticons.eu/

[30] Bjorgan, A., Milanic, M., & Randeberg, L. L. (2014). Estimation of skin optical parameters for real-time hyperspectral imaging applications. *Journal of biomedical optics*, *19*(6), 066003-066003.

[31] Milanič, M., Bjorgan, A., Larsson, M., Marraccini, P., Strömberg, T., & Randeberg, L. L. (2015, March). Hyperspectral imaging for detection of cholesterol in human skin. In *SPIE BiOS* (pp. 93320W-93320W). International Society for Optics and Photonics.

[32] Bjorgan, A., Denstedt, M., Milanič, M., Paluchowski, L. A., & Randeberg, L. L. (2015, March). Vessel contrast enhancement in hyperspectral images. In *SPIE BiOS* (pp. 93180G-93180G). International Society for Optics and Photonics.

[33] Milanic, M., Paluchowski, L. A., & Randeberg, L. L. (2015). Hyperspectral imaging for detection of arthritis: feasibility and prospects. *Journal of Biomedical Optics*, *20*(9), 096011-096011.

[34] Ferris, D. G., Lawhead, R. A., Dickman, E. D., Holtzapple, N., Miller, J. A., Grogan, S., ... & Faupel, M. L. (2001). Multimodal hyperspectral imaging for the noninvasive diagnosis of cervical neoplasia. Journal of Lower Genital Tract Disease, 5(2), 65-72.

[35] Panasyuk, S. V., Yang, S., Faller, D. V., Ngo, D., Lew, R. A., Freeman, J. E., & Rogers, A. E. (2007). Medical hyperspectral imaging to facilitate residual tumor identification during surgery. *Cancer biology & therapy*, *6*(3), 439-446.

[36] Bird, B., Remiszewski, S., Akalin, A., Kon, M., & Diem, M. (2012). Infrared spectral

histopathology (SHP): a novel diagnostic tool for the accurate classification of lung cancer. *Laboratory investigation*, *92*(9), 1358-1373.

[37] Kiyotoki, S., Nishikawa, J., Okamoto, T., Hamabe, K., Saito, M., Goto, A., ... & Sakaida, I. (2013). New method for detection of gastric cancer by hyperspectral imaging: a pilot study. *Journal of biomedical optics*, *18*(2), 026010-026010.

[38] Liu, Z., Wang, H., & Li, Q. (2011). Tongue tumor detection in medical hyperspectral images. Sensors, 12(1), 162-174.

[39] Huang, T. M., Kecman, V., & Kopriva, I. (2006). Kernel based algorithms for mining huge data sets (Vol. 1). Heidelberg: Springer.

[40] F. Molina, E. Prujá , R. Vera, M. Marcos, M. Tejedor, J. Albistur . Factores pronósticos en los tumores cerebrales. Anales. 2001. 24: suplemento 1.

[41] D. M. Muñoz Carmona, C. Faga Cantamessa, M. Márquez García-Salazar, J. Gómez Millán, E. Bayo. Nuevas perspectivas en el tratamiento paliativo del glioblastoma multiforme y astrocitoma anaplásico recidivado con implantes de carmustina. Oncología. 2005. 28: 5.

[42] Kleihues P. In Kleihues P, Cavenee WK. Pathology and genetics of tumours of the nervous system, World Health Organization classification of tumours. ISBN. 2000. 92-832-2409-4.

[43] Miguel Urtasun, Mariano Arrazola, José Angel Larrea, J.Villanúa, I. Ruiz, M. Lasa y cols.Protocolo en el tratamiento de los gliomas malignos. Kirurgia. 2006. 3.

[44] Van Meir, Hadjipanayis, C. G., Norden, A. D.,Shu, H. K., Wen, P. Y., Olson, J. J. Exciting New Advances in Neuro-Oncology: The Avenue to a Cure for Malignant Glioma. Cancer Journal for Clinicians. 2010; 60:166–93

[45] De Angelis LM. Brain Tumors. N Engl J Med. 2001;344:114-23.

[46] Roger Stupp. Fisher, WP. Mason, MJ van den Bent, M.Weller B. Fisher, MJ Taphoorn, et. al.Radiotherapy plus concomitant and adjuvant temozolamide for glioblastoma. N Engl J Med. 2005; 352:987-996.

[47] S. Ortega, G. M. Callicó, M. L. Plaza, R. Camacho, H. Fabelo and R. Sarmiento, "Hyperspectral database of pathological in-vitro human brain samples to detect carcinogenic tissues," *2016 IEEE 13th International Symposium on Biomedical Imaging (ISBI)*, Prague, 2016, pp. 369-372.

[48] Gillies, R., Freeman, J. E., Cancio, L. C., Brand, D., Hopmeier, M., & Mansfield, J. R. (2003). Systemic effects of shock and resuscitation monitored by visible hyperspectral imaging. *Diabetes technology & therapeutics*, *5*(5), 847-855.

[49] Callicó, G.M., Fabelo, H., Guerra, R., López, S., Ortega, S., Piñeiro, J.F., Szolna, A., Sarmiento, R., & Tejedor, M.. (2016). A Novel Use of Hyperspectral Images for Human Brain Cancer Detection using in-Vivo Samples. *BIOSTEC*.

[50] Witten, I. H., & Frank, E. (2005). Data Mining: Practical machine learning tools and techniques. Morgan Kaufmann.

[51] Camps-Valls, G., & Bruzzone, L. (2005). Kernel-based methods for hyperspectral image classification. Geoscience and Remote Sensing, IEEE Transactions on, 43(6), 1351-1362.

[52] Chang, C. C., & Lin, C. J. (2011). LIBSVM: a library for support vector machines. ACM Transactions on Intelligent Systems and Technology (TIST), 2(3), 27.

[53] Benediktsson, J. A., Palmason, J. A., & Sveinsson, J. R. (2005). Classification of hyperspectral data from urban areas based on extended morphological profiles. Geoscience and Remote Sensing, IEEE Transactions on, 43(3), 480-491.

[54] Akbari, H., Kosugi, Y., Kojima, K., & Tanaka, N. (2008). Wavelet-based compression and segmentation of hyperspectral images in surgery. In Medical Imaging and Augmented Reality (pp. 142-149). Springer Berlin Heidelberg.

[55] Blanco, F., López-Mesas, M., Serranti, S., Bonifazi, G., Havel, J., & Valiente, M. (2012). Hyperspectral imaging based method for fast characterization of kidney stone types. Journal of biomedical optics, 17(7), 0760271-07602712.

[56] Dietterich, T. G. (2000). Ensemble methods in machine learning. In Multiple classifier systems (pp. 1-15). Springer Berlin Heidelberg.

[57] Chan, J. C. W., & Paelinckx, D. (2008). Evaluation of Random Forest and Adaboost tree-based ensemble classification and spectral band selection for ecotope mapping using airborne hyperspectral imagery. Remote Sensing of Environment, 112(6), 2999-3011.

Annex I

HYPERSPECTRAL DATABASE OF PATHOLOGICAL IN-VITRO HUMAN BRAIN SAMPLES TO DETECT CARCINOGENIC TISSUES

S. Ortega[1], G. M. Callicó[1], M. L. Plaza[2], R. Camacho[2], H. Fabelo[1], R. Sarmiento[1]

[1]Institute for Applied Microelectronics, University of Las Palmas de Gran Canaria, Spain

[2]University Hospital Doctor Negrín of Las Palmas de Gran Canaria, Spain

ABSTRACT

Hyperspectral imaging is an emerging technology for medical diagnosis. Some previous studies have used this type of images to detect cancer diseases. In this research work, a multidisciplinary team conformed by pathologists and engineers has created a diagnosed hyperspectral database of in-vitro human brain tissues. In order to capture the hyperspectral information from histological slides, an acquisition system based on a microscope coupled with a hyperspectral camera has been developed. Preliminary results of applying two different supervised classification algorithms (Support Vector Machines and Artificial Neural Networks) to the hyperspectral database show that an automatic discrimination between healthy and tumour brain tissues from in-vitro samples is possible using exclusively their spectral information. The sensitivity and the specificity are over 92% in all the cases.

***Index Terms*—** Brain cancer detection, Hyperspectral imaging, Data mining, Support vector machine, Artificial neural network

1. INTRODUCTION

Hyperspectral Imaging (HSI) is a technology that combines both spectroscopy and digital imaging, measuring hundreds of narrow bands from the electromagnetic spectrum. Each material has its own interaction with radiation, which can be measured either by using the reflectance or the absorbance values. The response to different wavelengths for a single material is called spectral signature, which allows the discrimination between different types of materials. The data structure used by HSI systems is called hypercube, and it stores all the spatial and spectral information enclosed in a scene. There are a few types of hyperspectral cameras, depending on the way that they capture the hypercubes. In this research work, a pushbroom camera was used. This type of camera is based in an optical element called spectrograph, used for splitting the light into narrow wavelength bands. Each hyperspectral image taken by a pushbroom camera involves the capture of a two dimensional image which contains all the spectral information, but it only captures one-dimensional spatial information (a single line) from a surface. In order to generate a full hypercube, it is necessary to incorporate a linear-scan system, where either the camera or the sample to be captured must be moved synchronously.

Although HSI has been widely used in Remote Sensing, it is an emerging technology for clinical diagnosis. Some studies have proven that interaction between electromagnetic radiation and tissue carries useful information for diagnosis proposals [1]. A variety of studies shows that HSI is a helpful tool in the diagnosis of several cancer diseases. Some studies about prostate [2], ovaries [3], breast [4], and tongue [5] cancer detection using HSI have been recently published.

Hyperspectral imaging involves managing a large amount of data, so in order to extract relevant information from the hypercubes, a data mining process is required. In the studies previously reviewed, some supervised classification algorithms have been used. Support Vector Machines (SVM) [6] is a kernel-based supervised classification technique which has been widely used in the classification of medical hyperspectral images [1]. Artificial Neural Network (ANN) is another machine learning approach also used in medical applications, being multilayer perceptron (MLP) the most popular type of Neural Network [7]. In this paper both approaches will research if an automatic discrimination between tumour and healthy brain tissues can be performed using hyperspectral imaging.

2. METHODS

2.1. Description of biological samples

The biological samples used in this research work consist in biopsies of human brain tissue resected during surgery. A sample of the tumour's tissue is required for the pathologic diagnosis during or after the surgery. A biopsy is the removal of a small amount of tissue for the examination under a microscope and is the conclusive way that a brain tumour can be trustworthy diagnosed. The sample removed during the biopsy is analysed by a pathologist. A biopsy can be done as part of a surgery to remove the entire tumour or as a separate procedure if surgical removal of the tumour is not possible because of its location or patient's health. This biopsy has followed a histological processing, whereby tissue specimens are prepared for sectioning, staining and diagnosis. Once biopsy has been diagnosed, tissue is sorted according to the Wold Health Organization (WHO) classification of tumours of the nervous system.

In this study, 4 different patients were used, and 13 diagnosed pathology slides were available. Pathology slides were provided by the Anatomy Pathology department of Doctor Negrín Hospital, at Las Palmas of Gran Canaria. In order to facilitate the labelling process of the hyperspectral data, once pathologists had a diagnosis for a certain tissue, they marked the regions of interest in the slide with a coloured pen. Tumour tissues were marked with red colour, and healthy tissues were marked using blue colour (Fig. 1).

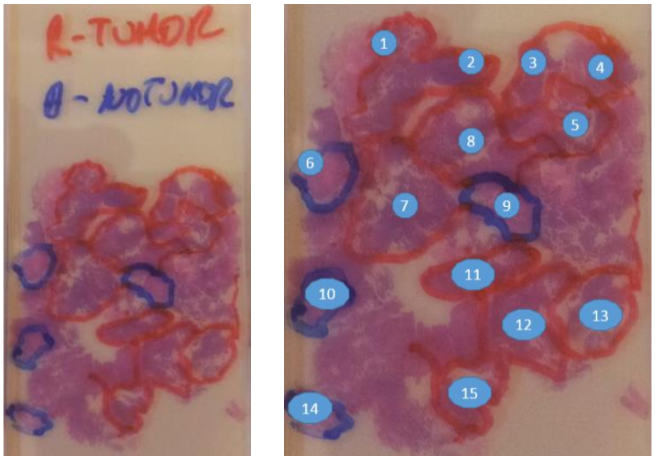

(a) (b)

Fig. 1. (a) One of the diagnosed histological slides used in this study (b) Location of the hypercubes in a histological slide

2.2. Instrumentation

In order to register hyperspectral images from pathology slides, a capture system consisting on a HSI camera coupled with a microscope has been developed (Fig. 2.a). The hyperspectral camera used was the *Specim ImSpector VNIR V10-E*, which works in the VNIR spectral range (from 400 nm to 1000 nm) with a spectral resolution of 2.8 nm. It is a pushbroom camera, so to capture a whole hypercube, either the camera or the sample must be moved synchronously with the shoot of the camera. The Microscope used was the *Olympus BH2-MJLT*. With this microscope it is possible to do observations by transmittance or reflectance of light in tissue, with magnifications of 5x, 10x, 20x, 50x and 100x. It has its own source of light which consists in a power-adjustable halogen bulb (*Philips CAPSUline PRO 13102*). This light has been tested to emit in all the frequency range previously mentioned.

So as to obtain a hypercube from the pathology slides, a linear-movement mechanism has been employed. This mechanism is based on a *Sony PlayStation 3* (PS3) Blue-Ray reader driver, with a movement resolution of 9 µm. This mechanism is synchronized with the capture of each pushbroom line of the camera. A full custom C++ based software has been developed to control both the camera and the mechanism movement.

In order to attach the linear-movement mechanism into the microscope, a wooden flat platform has been built and replaced by the original plate of the microscope (Fig. 2.b). The slides are coupled to the PS3 driver using permanent magnets (Fig. 2.c). A Graphical User Interface (GUI) has been developed to provide users an easy-to-use interface which encapsulates the complexity of the capture system in a single button.

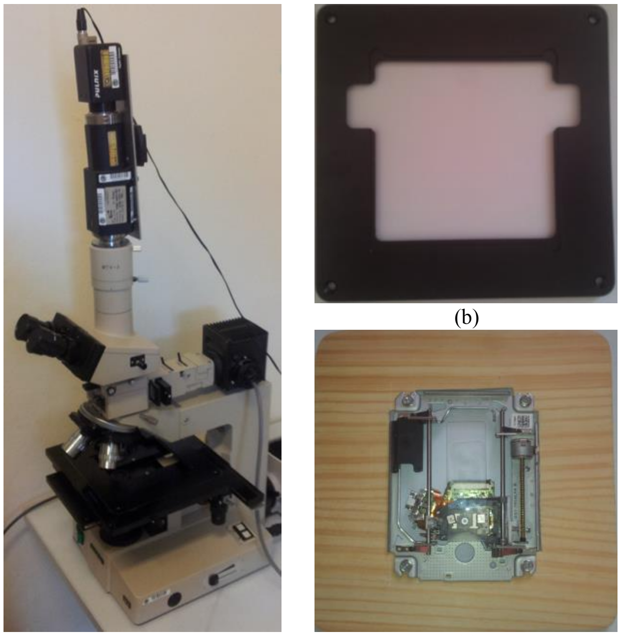

(b)

(a) (c)

Fig. 2. (a) Acquision system based on a microscope coupled with a hyperspectral camera (b) Original microscope plate (c) Customized microscope plate with the linear-movement mechanism attached.

The following conclusions were reached from the test of the acquisition system developed:

1) When coupling the microscope with the HSI camera, the pushbroom line captured width is 4.4 µm using 5x magnification and 2.2 µm with 10x magnification. Due to the resolution of the stepper motor, which is of 9 µm, the collected hypercubes have some missing spatial information between each pushbroom lines captured.

2) It has been found that the microscope heavily filters the wavelengths above 800 nm.

3) Hypercubes have only been captured using the transmittance observation mode and only with 5x and 10x magnifications. The sensitivity of the HSI camera sensor does not allow making observations neither with reflectance observation technique nor using the other lenses available. This is because the power of the light source used is not bright enough to make measures in the reflection mode or with higher magnification lenses.

2.3. Database creation

Using the HSI capture system described in section 3, the procedure of capturing hypercubes has been quite automatic. Firstly, the focus should be done through the microscope binocular, ensuring that the HSI pushbroom image is also focused. Then, the capture starts when the capture button is pressed in the capturing GUI previously described. In order to keep a correspondence between the pathology slides and the captured hypercubes, a labelling of the regions of interest is performed. Each region of interest of the slides is enumerated, and an identification number is assigned to each hypercube (Fig. 1.b).

The goal of this study was collecting a labelled spectral dataset of pathological samples in order to figure out if HSI could be used as a helpful diagnosis tool for this type of diseases. The chromatic dye employed in this work equally stains both healthy and tumour tissues. Diagnosis of neoplasia is accomplished accordingly to the morphological comparison between different types of tissues, cells and stroma. The use of visual colour by itself does not provide enough information for pathological diagnosis. To tag each spectra as *healthy* or *tumour* according to the diagnostic given by the pathologist, a new GUI was developed. In this new GUI, a synthetic RGB image (Fig. 3.a) is shown, and the user must crop a region of interest that only contains diagnosed tissue. Once a region of the image has been selected, a dialog window is shown and the user must introduce if the region of interest is healthy (marked as blue by pathologist) or tumour (marked as red). Subsequently, the spectra of the selected pixels are extracted from the hypercube and the labels are added to the pathological hyperspectral dataset.

To provide the user with a synthetic RGB image, wavelengths near red (650 nm), green (550 nm) and blue (420 nm) are averaged in order to generate the red, green and blue channels of a normal RGB image. Additionally, the images are processed to discriminate between useful pixels (tissue) and background pixels (microscope light). A binarization of the RGB image is done in order to achieve the identification of tissue pixels in the hypercube (Fig. 3.b). The threshold that better separates the background from the tissue was determined by means of several experiments.

A dataset of 83 hypercubes has been obtained for each optical magnification (5x and 10x) after capturing all the samples (166 in total). By extracting and labelling the spectral data from these hypercubes, a dataset of approximately 12 million spectra was generated (only for 5x magnification), where 15% of the spectra belongs to *healthy* tissue. Fig. 4 shows the mean of *healthy* tissue (blue) and *tumour* tissue (red) hyperspectral signatures.

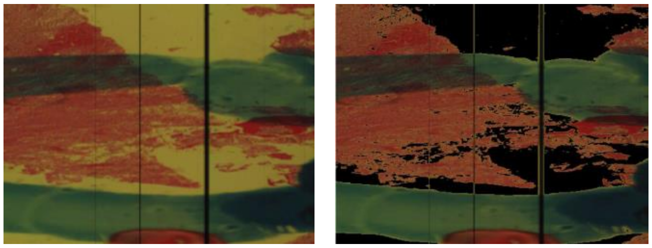
(a) (b)

Fig. 3. (a) Synthetic RGB image extracted from a hypercube (b) Separated tissue and background using binarization.

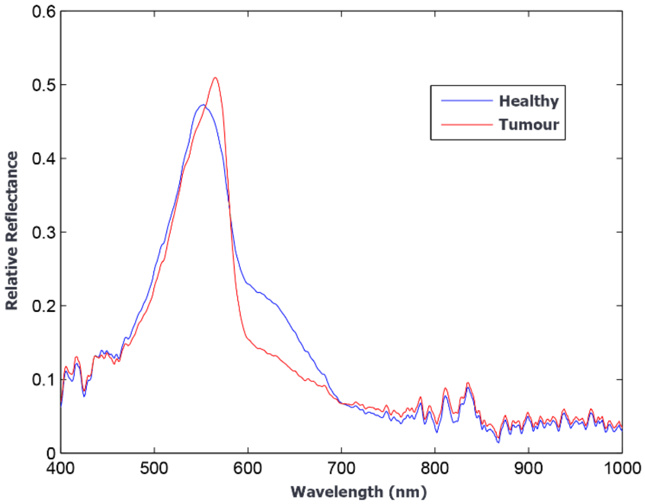

Fig. 4. Mean values of hyperspectral signatures of the *healthy* tissue and *tumour* tissue, ranging from 400 nm to 1000 nm.

3. EXPERIMENTAL RESULTS

The created database has been classified using a *machine learning* chain in order to determine if it is possible to distinguish between healthy tissue and tumour tissue using only its spectral information. Table I shows the preliminary results of the classification using SVM and ANN. In order to test both classification models, a randomly-selected set of spectra was taken from the database. Then, this dataset has been split into *training data* and *test data* in order to perform hold-out validation. These preliminary results were obtained using 40,000 samples, where 25% were *training samples* and 75% *test samples*.

After testing several configurations for the selected classification algorithms, some conclusions have been reached. For SVM, it has been proven that a linear kernel provides a performance as accurate as other more complex kernels (like polynomial or Gaussian) with a lower computational cost. In the same way, several neural networks architectures varying the number of hidden layers, the number of neurons inside this layers and the activation function selected for each layer have been tested. The experimental results shown that the best performance is obtained using a multilayer neural network with a single hidden layer with 33 neurons, using a logistic activation function for this layer. A hyperbolic tangent sigmoid activation function has been selected for the output layer.

In this work, the following standard metrics have been used in order to evaluate the classification results:

- **Sensitivity:** relates to the tests ability to identify a condition correctly. It is obtained as the number of true positives divided by the total number of true positives and false negatives in population (see equation 1).
- **Specificity:** relates to the tests ability to exclude a condition correctly. It is obtained as the number of true negatives divided by the total number of true negatives and false positives in population (see equation 2).

The results presented in Table I reveal that the specificity and the sensitivity of distinguishing between tumour tissue and healthy tissue is over 92 % using any of the proposed classifiers. The coherence between sensitivity and specificity means that both classes (tumour and healthy) are both correctly classified. These results were obtained without the use of exhaustive pre-processing chain before classifying, which probably would increase the quality of the classifiers performance.

$$Sensitivity\ (\%) = 100 \cdot \frac{TP}{TP + FN} \qquad (1)$$

$$Specificity\ (\%) = 100 \cdot \frac{TN}{TN + FP} \qquad (2)$$

TABLE I PRELIMINARY CLASSIFICATION RESULT USING SVM AND ANN

Classification Algorithm	Specificity	Sensitivity
SVM	92.61 %	94.44 %
ANN	92.44 %	92.77 %

4. CONCLUSIONS

It has been shown that the developed acquisition system is capable to register hyperspectral data contained in biological preserved slides. This system has been used to generate a database of human in-vitro brain tissues labelled as *healthy* or *tumour* tissues. Preliminary results show that it is possible to discriminate between healthy and tumour tissues by exclusively processing the spectral information of the tissue.

The on-going work in this research is to increase the database to include new patients. Another task to be done is to define a new set of more-detailed labels according to a more complex pathology diagnosis (for example, defining tumour types depending on its grade). This kind of studies could show the capability of HIS in automatic detection of cancer diseases from pathological slides.

As far as the acquisition system is concerned, the capture system could be improved. In section 3, the weaknesses of the acquisition system were outlined: i) there is some missing spatial information due to the linear-movement mechanism resolution; and ii) the light source is not powerful enough to allow capturing hyperspectral information using reflectance observation methods. Using a mechanism with a higher resolution, a whole hypercube from pathology slides (with no gaps between the pushbroom lines) could be obtained. Furthermore, a higher power light source could allow making tissue registrations with all the available lenses and also in reflectance observation mode.

Finally, the data mining process performed must be improved in order to extract as much information as possible from the available spectral database. This task involves pre-processing of data, dimensional reduction, feature selection and testing new supervised classification algorithms.

5. ACKNOWLEDGMENT

This work has been supported in part by the European Commission through the FP7 FET Open programme ICT-2011.9.2, European Project HELICoiD "HypErspectral Imaging Cancer Detection" under Grant Agreement 618080.

6. REFERENCES

[1] Lu, Guolan, and Baowei Fei. "Medical hyperspectral imaging: a review." *Journal of biomedical optics* 19.1 (2014): 010901-010901

[2] Akbari, Hamed, et al. "Hyperspectral imaging and quantitative analysis for prostate cancer detection." *Journal of Biomedical Optics* 17.7 (2012): 0760051-07600510.

[3] Akbari, Hamed, et al. "Cancer detection using infrared hyperspectral imaging."*Cancer science* 102.4 (2011): 852-857.

[4] Panasyuk, Svetlana V., et al. "Medical hyperspectral imaging to facilitate residual tumor identification during surgery." *Cancer biology & therapy* 6.3 (2007): 439-446.

[5] Liu, Zhi, Hongjun Wang, and Qingli Li. "Tongue tumor detection in medical hyperspectral images." *Sensors* 12.1 (2011): 162-174.

[6] Kecman, Vojislav. *Learning and soft computing: support vector machines, neural networks, and fuzzy logic models*. MIT press, 2001.

[7] Haykin, Simon S., et al. *Neural networks and learning machines*. Vol. 3. Upper Saddle River: Pearson Education, 2009.